

Review

A comprehensive review and outlook of bifacial photovoltaic (bPV) technology

Wenbo Gu^a, Tao Ma^{a,*}, Salman Ahmed^a, Yijie Zhang^a, Jinqing Peng^b^a School of Mechanical Engineering, Shanghai Jiao Tong University, Shanghai, China^b College of Civil Engineering, Hunan University, Changsha, Hunan, China

ARTICLE INFO

Keywords:
 Bifacial photovoltaic (bPV)
 Modelling
 Experimental study
 Performance characterization
 Applications

ABSTRACT

Bifacial photovoltaic (bPV) technology is regarded as a promising alternative, as it can generate more power than conventional mono-facial PV (mPV) technology by absorbing sunlight from both sides. However, reviews on bPV are limited. Challenges, such as complex mechanisms, non-uniform rear-side irradiance and other issues constrain the bPV development. Therefore, it is necessary to present an overview on recent bPV development from various perspectives and provide some potential directions for future research. Therefore, an overview of bPV is demonstrated in this study, including its working principle, basic structure, cell categories, energy losses, merits and demerits. Moreover, recent research on bPV technology is discussed with respect to numerical modelling, software simulation, experimentation, economics, involved parameter analyses, performance characterization and system applications. Finally, some future perspectives and potential approaches are proposed for future research and to make bPV technology more cost-effective and competitive, since the current levelized cost of energy of bPV is only 2–6% lower than conventional mPV systems.

1. Introduction

The Earth has already been considered as a planet that is facing energy crisis, global warming and air pollution since the beginning of electrification era [1,2]. Faced with these challenges, utilization of renewable energy resources has been proposed as a sustainable alternative, especially photovoltaic (PV) systems due to the abundance of solar energy [3,4]. The global PV industry has expanded excessively in the past decade, with around 505 GW of global PV circulative installation by 2018 [5]. Future research will focus on system optimization and cost reduction associated with grid parity, which is specifically considered by China's 531 New Policy [6,7].

Under these circumstances, the interest in crystalline silicon cells within the market and academic circles has shifted from mono-facial PV (mPV) technology to bifacial PV (bPV) technology, increasing from less than 20% in 2019 to 70% in 2030 as presented in Fig. 1 [8,9].

The bPV technology seems to be a novel concept, but the first work done on bPV technology can be traced back to a patent issued by Hiroshi in 1966 [10]. The first bifacial lab cell was fabricated and exhibited in 1977 [11], followed annually with few articles about high efficiency and real applications [12,13] as presented in Fig. 2.

It can be seen that articles about bPV technology began increasing from 2009, as researchers started working on this novel technology on a global stage, especially from countries that were already major players in the PV industry such as China, USA, Germany and Japan as shown in Fig. 3. Mathematical models were explored. The bPV power output estimated by Sun et al. [14] is 30% higher than mPV when the albedo is 0.5 and the elevation is 1 m. Not only is the power output greater, specific properties of bPV technology contributes to 2–6% lower Levelized Cost of Energy (LCOE) [15] when the latitude is higher than 30°. The concept of LCOE was also employed by Rodríguez-Gallegos et al. [16] from a global prospective to recommend bPV as a more cost-effective PV technology under two conditions: 1) latitudes above 40° in spite of albedo; 2) latitudes below 40° but with high albedo (higher than 0.12–0.30 depending on locations). In addition, some experiments were also undertaken to estimate the bPV performance [17]. Stein et al. [18] employed bPV modules in convectional PV systems under many kinds of configurations, such as different tilts, heights, orientations, and track methods. Results show that bPV modules outperform mPV and perform better with the increment of albedo and the reduction of ground shading. An outdoor bPV experiment also conducted by Wei et al. [19] shows that high albedo is beneficial to get high power output gain, up to 15% and 30% on sandy and snowy land, respectively. Numerous

* Corresponding author.

E-mail address: tao.ma@connect.polyu.hk (T. Ma).

| Nomenclature | |
|-----------------------|---|
| Abbreviations | |
| AMO | any module orientation |
| anti-PID | anti-potential induced degradation |
| BIPV | building integrated photovoltaics |
| bPV | bifacial photovoltaic |
| BSF | back surface field |
| DC | down conversion |
| DHI | diffuse horizontal irradiance |
| DSBCSC | double-sided buried contact solar cell |
| EVA | ethylene-vinyl acetate copolymer |
| GHI | global horizontal irradiance |
| HIT | heterojunction with intrinsic thin-layer |
| IBC | interdigitated back contact |
| ISS | International Space Station |
| LCOE | levelized cost of energy |
| MPP | maximum power point |
| mPV | mono-facial photovoltaics |
| NREL | National Renewable Energy Laboratory |
| NRMSD | normalized root mean square deviation |
| PERC | passivated emitter rear contact |
| PERL | passivated emitter rear locally-diffused |
| PERT | passivated emitter rear totally diffused |
| POE | ethylene-octene copolymer |
| PV | photovoltaic |
| PV/T | photovoltaic/thermal |
| QDs | quantum dots |
| SAM | system advisor model |
| UC | up conversion |
| VMO | vertical module orientation |
| Symbols | |
| <i>a</i> | coefficient considering the effect of circumsolar incident angle on the diffuse irradiance of tilted panel |
| <i>A</i> | area (m^2) |
| <i>b</i> | coefficient considering the effect of circumsolar incident angle on the diffuse irradiance of horizontal panel |
| <i>BG_E</i> | additional bifacial energy gain (%) |
| <i>C_n</i> | net costs in year <i>n</i> (USD) |
| <i>d</i> | degradation rate |
| <i>E_g</i> | band gap (eV) |
| <i>E_n</i> | actual electricity generation in year <i>n</i> (kWh) |
| <i>F₁</i> | condition of circumsolar brightness |
| <i>F₂</i> | condition of horizontal brightness |
| <i>F_n</i> | interest expenditures in year <i>n</i> (USD) |
| <i>G</i> | irradiance (W/m^2) |
| <i>G₀</i> | global irradiance outside the atmosphere (W/m^2) |
| <i>h</i> | normalized clearance height, $h = H_p/CW$, where H_p is the clearance height of the PV panel and CW is the PV collector width. |
| <i>I₀</i> | reserve saturation current of the diode (A) |
| <i>I_n</i> | initial investment in year <i>n</i> (USD) |
| Subscripts | |
| <i>a</i> | ambient |
| <i>b</i> | beam |
| <i>c</i> | photovoltaic cell |
| <i>d</i> | diffuse |
| <i>mpp</i> | maximum power point |
| <i>r</i> | reflection |
| <i>ref</i> | reference conditions, i.e. standard test conditions |
| <i>sgrd</i> | shaded ground |
| <i>usgrd</i> | unshaded ground |
| Greek symbols | |
| α | absorptivity |
| α_{sc} | temperature coefficient of short circuit current ($^{\circ}/\text{C}$) |
| β_{ref} | temperature coefficient of open-circuit voltage under standard test conditions ($\text{V}/^{\circ}\text{C}$) |
| η | energy efficiency |
| β_p | tilt angle of the photovoltaic module |
| ρ_p | ground albedo |

research studies, including simulation and experiments, about bPV technology have been done in scientific circles. However, technology reviews on bPV are quite limited. In addition, some challenges, such as non-uniform rear-side irradiance constrains the development of bPV technology. Therefore, it is necessary to present an overview on recent bPV development from various perspectives and provide some potential directions for future research.

This paper, which is divided into 5 sections, presents a comprehensive review and outlook of the bPV technology in order to help the

researchers interested in this field to thoroughly understand this novel technology. Section 2 gives an overview of the bPV technology. Section 3 illustrates the performance of such systems with reference to mathematical models, computer simulations, experimental tests, economic factors, parametric analysis, testing methods and practical applications. Challenges faced by bPV systems are presented in Section 4, followed by some potential approaches and future perspectives. Finally, a brief summary of the study is given in Section 5.

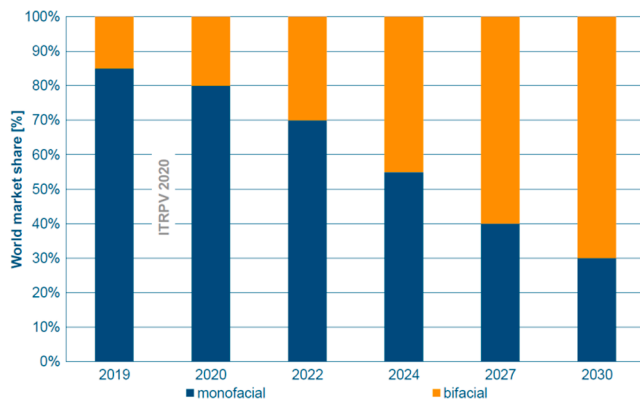


Fig. 1. The development trend of PV market [8].

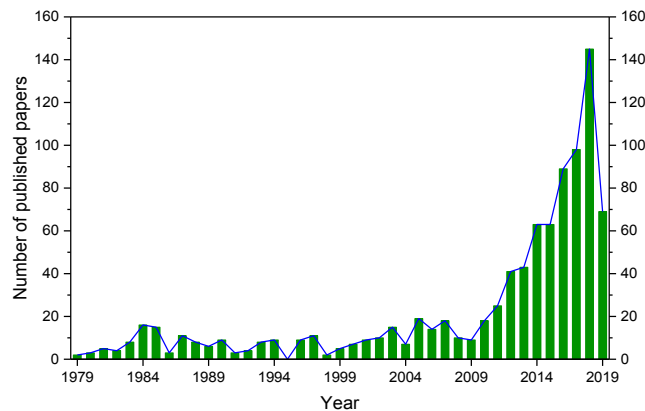


Fig. 2. Articles published about bPV technology from 1979 to Aug., 2019 (Source: Scopus).

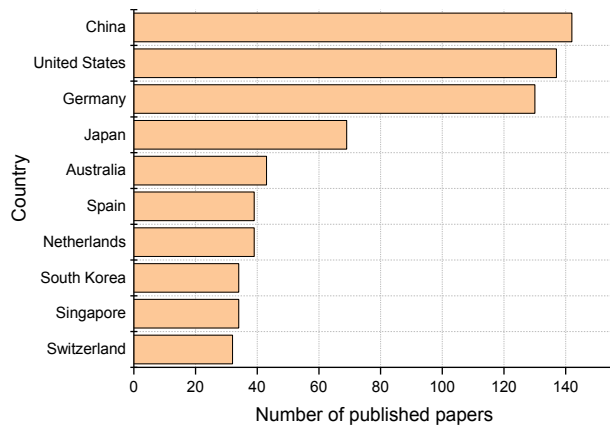


Fig. 3. Top 10 publishing countries for bPV technology papers until August 2019 (Source: Scopus).

2. Overview of bPV technology

2.1. General principle

Bifacial PV technology has a similar working principle as mPV, namely photoelectric effect. Compared to mPV, bPV cells add a layer of anti-reflection coating and back contacts instead of the back surface field (BSF) at the back side of PV cells. This is due to the property of absorbing sunlight from both sides as presented in Fig. 4. When solar cells are exposed to the sun, light transmits through the anti-reflection coatings

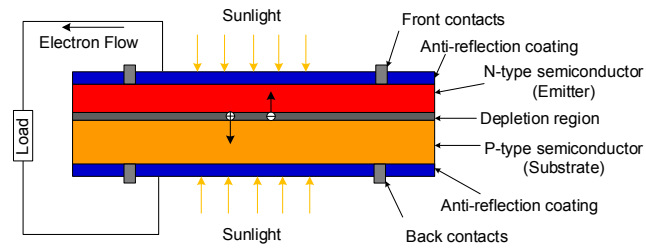


Fig. 4. Schematic of bPV technology.

from both sides of the PV cells. The photons with higher energy than the band gap transfers part of their energy to electrons to form electron-hole pairs [20]. Carriers generating near the depletion region inside the semiconductor are not recombined but diffuse to the substrate and emitter. The carriers are then attracted by the internal electric field, causing electrons to flow into the N-type semiconductor and holes to flow into the P-type semiconductor. As a result, an electromotive force generates between the front and back contacts. Electrons flow through the external load once both sides of the PV cells are connected.

2.2. Basic structure

As a novel technology, due to the property of receiving sunlight, there is one layer of anti-reflection coating on the back of the junction instead of a back surface field as presented in Fig. 5. Therefore, the front appearance is very similar to the rear one.

2.3. Cell categories

2.3.1. Manufacturing processes

With the increasing demand of highly efficient PV cells, various bifacial modules based on bPV technology with different manufacturing processes are available in the PV market. These include passivated emitter rear contact (PERC), passivated emitter rear locally-diffused (PERL), passivated emitter rear totally diffused (PERT), heterojunction with intrinsic thin-layer (HIT), interdigitated back contact (IBC) and double-sided buried contact solar cell (DSBCSC) [6]. A basic view of each module can be seen in Fig. 6. The differences of structure results in various bifaciality coefficient ranges for these PV cells: 70–80% (PERC, IBC and DSBCSC); 80–85% (PERL and PERT); 95–100% (HIT), indicating that HIT can generate more power output under the same conditions.

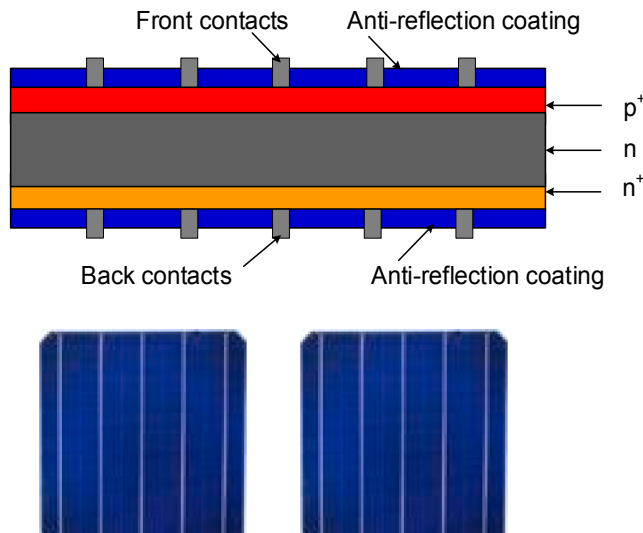


Fig. 5. Bifacial PV cell structure and appearance [21].

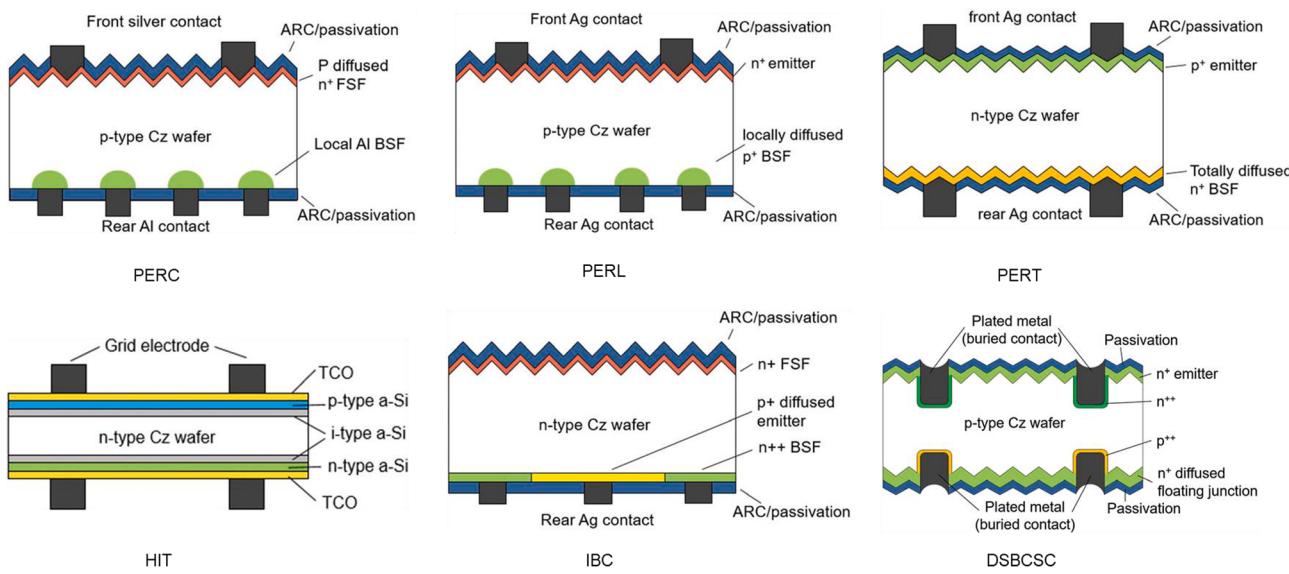


Fig. 6. Various bPV structures [6].

2.3.2. Backsheet materials

Bifacial PV modules in the PV market have two different backsheets, namely glass and transparent organic material, whose characterizations are listed in Table 1. Different materials with different characterizations provide the PV market with selective chance under various conditions.

2.4. Energy losses

The bPV module can produce electricity from both sides by absorbing a part of the sunlight, while the rest is dissipated as energy losses in the cell and from the cell to the module (Fig. 7) [26]. The losses from the cell to the module is categorized as interconnection reflection and resistance [27,28]. The losses in the cell can be divided into three groups according to carrier lifetime, namely generation, transportation and recombination processes [29]. More details can be found in Refs. [30,31].

2.5. Merits and demerits

Due to the property of absorbing sunlight from both sides, this special structure contributes to 5–30% more power output and 2–6% lower LCOE [15], despite the complex manufacturing, installation and design with the risk for more shade of back side. In addition, conventional organic backsheets suffers from pulverization, because of the exposure to ultraviolet rays from the ground, and experiences functional failure from the gaps and intrusions of water vapor [24,25]. The glass-glass structure of the bPV modules contributes to a lower cleaning frequency [32] and longer lifetime, than mpV modules that have the traditional glass-organic backsheets structure [22], because of lower cell temperature [26,33] and stronger endurance to unfavorable environment [14].

Table 1
Characterizations of bPV backsheets materials.

| Materials | Characterizations |
|------------------------------|---|
| Glass | <ul style="list-style-type: none"> Long durations under unfavorable environmental conditions [14,22] Durable waterproof performance Strong anti-potential induced degradation (anti-PID) [23–25] |
| Transparent organic material | <ul style="list-style-type: none"> Low weight Strong anti-soiling ability Low cell-to-module current loss |

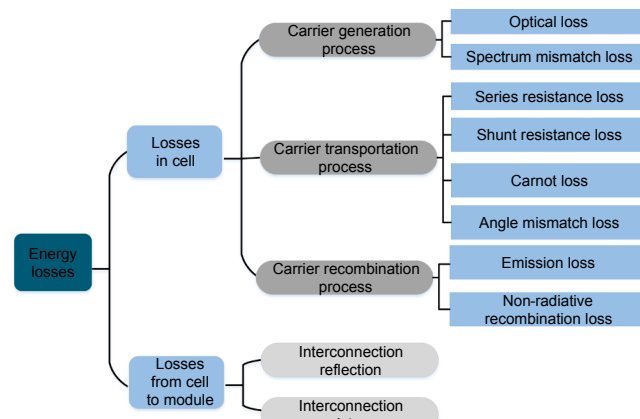


Fig. 7. Various energy losses in a bPV module.

Furthermore, bPV modules can be used in wider applications, such as noise barriers [34] and building facades [35], due to insensitivity towards orientation and inclination.

3. Comprehensive review on bPV technology

In this section, a detailed review of bPV technology in the literature is done with respect to mathematical modelling, software simulation, experimental tests, economic issues, various parameters analysis, testing methods and practical applications.

3.1. Performance modelling of bPV modules

To estimate the performance of bPV modules, it is vital to develop some mathematical models, namely the optimal model, electrical model and thermal model, with a framework for simulating the bPV performance as presented in Fig. 8 [21]. Onsite weather parameters, including global horizontal irradiance (GHI), diffuse horizontal irradiance (DHI), ambient temperature (T_a) and wind velocity (u_w), which can be obtained from some meteorological data companies, such as SolarGIS [36] or estimated simply from clear sky model [37]. Installation parameters consist of tilt angle (β_p), azimuth angle (γ_p), elevation (E_p) and albedo (ρ_p).

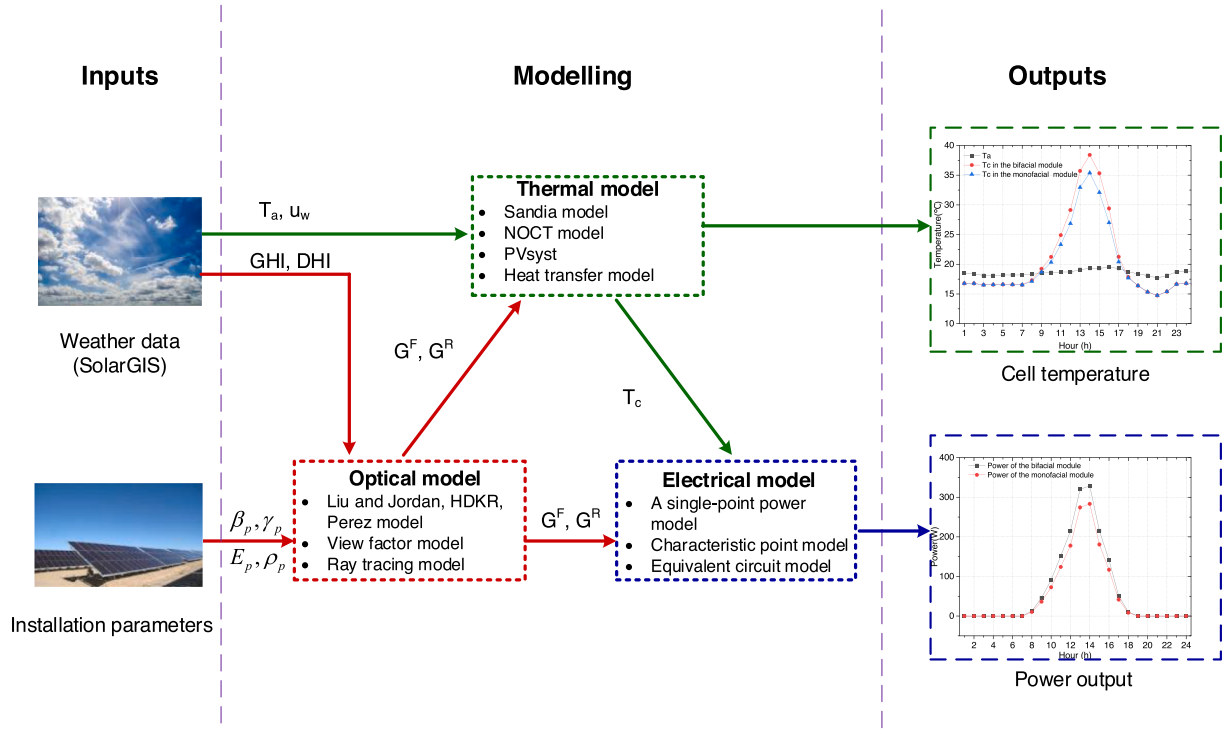


Fig. 8. A framework for simulating the bPV performance [21].

Weather and installation parameters are input into the optical model to calculate the front- and rear-side irradiances, which are combined with ambient temperature T_a and wind velocity u_w in thermal model to obtain cell temperature T_c . Combined together, the outputs of the optical model and thermal model are fed as input to the electrical model, and lastly the module power output can be obtained [14].

3.1.1. Optical modelling

A bPV module can absorb a part of the sunlight to generate electricity with various optical losses. These optical losses occur at different interfaces on both sides, including reflection loss, absorption loss and transmittance loss [38] as presented in Fig. 9. Therefore, it is significant to appropriately obtain the irradiances of the bPV module from both the front and the rear sides.

3.1.1.1. Front-side irradiance.

The tilted front-side global irradiance G^F

can be obtained as Eq. (1):

$$G^F = G_b^F + G_d^F + G_r^F = (GHI - DHI) \cdot R_b^F + G_d^F + GHI \cdot \rho_p \cdot \frac{1 - \cos\beta_p}{2} \quad (1)$$

where the superscript 'F' means front side, G_b , G_d and G_r are three parts of the global tilted irradiance, namely beam, diffusion and reflection, β_p is the tilt angle of the PV module, ρ_p is the ground albedo and R_b^F is the ratio of front tilted irradiance and horizontal irradiance [21].

Diffuse irradiance is more complicated than beam and reflected irradiances and it has attracted researchers to work on models, such as the Liu and Jordan model, HDKR model and Perez model.

(a) Liu and Jordan model

Liu and Jordan model [39] is a represent of the isotropic model, which is defined as Eq. (2):

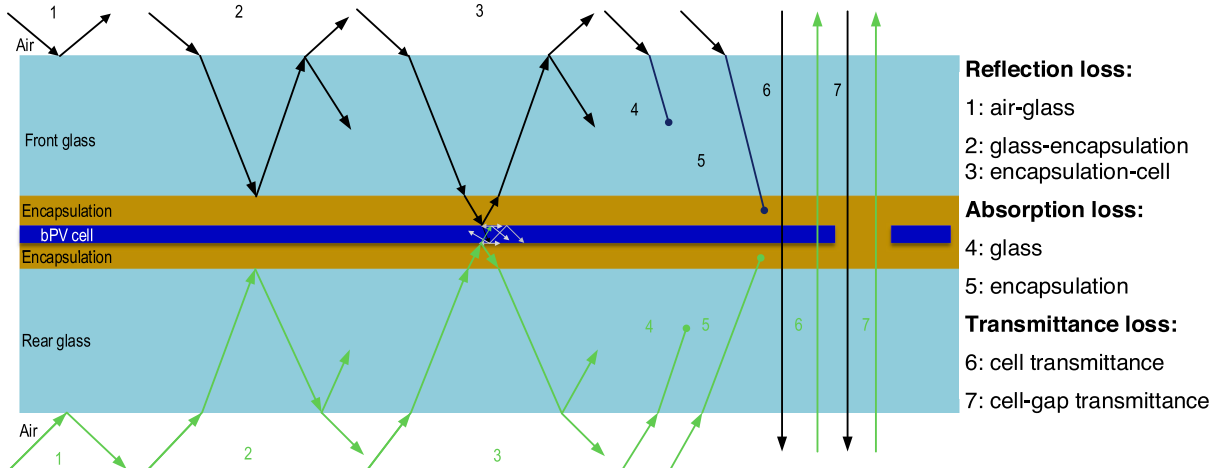


Fig. 9. Optical losses for a typical bPV module.

$$G_d^F = DHI \cdot \left(\frac{1 + \cos\beta_p}{2} \right) \quad (2)$$

(b) HDKR model

Hay, Davies, Klucher and Reindl put forward their equations to improve the isotropic model, respectively, which were combined as HDKR model as presented in Eq. (3) [40]:

$$G_d^F = DHI \cdot \frac{(GHI - DHI)}{G_0} \cdot R_b^F + DHI \cdot \left(1 - \frac{(GHI - DHI)}{G_0} \right) \left(\frac{1 + \cos\beta_p}{2} \right) \left[1 + \sqrt{\frac{(GHI - DHI)}{GHI}} \sin^3\left(\frac{\beta_p}{2}\right) \right] \quad (3)$$

where G_0 is the global irradiance outside the atmosphere.

(c) Perez model

Perez et al. [41] proposed a so-called Perez model to estimate the tilted diffuse irradiance, consisting of horizontal brightening, circumsolar diffuse and sky isotropic diffuse irradiances as presented in Eq. (4):

$$G_d^F = DHI \cdot (1 - F_1) \left(\frac{1 + \cos\beta_p}{2} \right) + F_1 \frac{a}{b} + F_2 \sin\beta_p \quad (4)$$

where a and b represent the coefficients considering the effect of circumsolar incident angle on the diffuse irradiance of the tilted and horizontal panels, F_1 and F_2 present the conditions of circumsolar brightness and horizontal brightness [41].

To summarize, isotropic models and the related parameters are quite easy to calculate, but not as accurate as anisotropic models, especially the Perez model, under most conditions.

3.1.1.2. Rear-side irradiance. For rear-side irradiance modelling, there are two common methods to achieve the goal, namely view factor model and ray tracing, which will be introduced in detail.

(a) View factor model

View factor is a rather important concept in calculation of rear-side irradiance. For a specific bPV module with a height of H_p , elevation of E_p and tilt angle of β_p , there are three view factors ($X_{R,sky}$, $X_{R,usgrd}$ and $X_{R,unsgd}$) for rear panel as presented in Fig. 10.

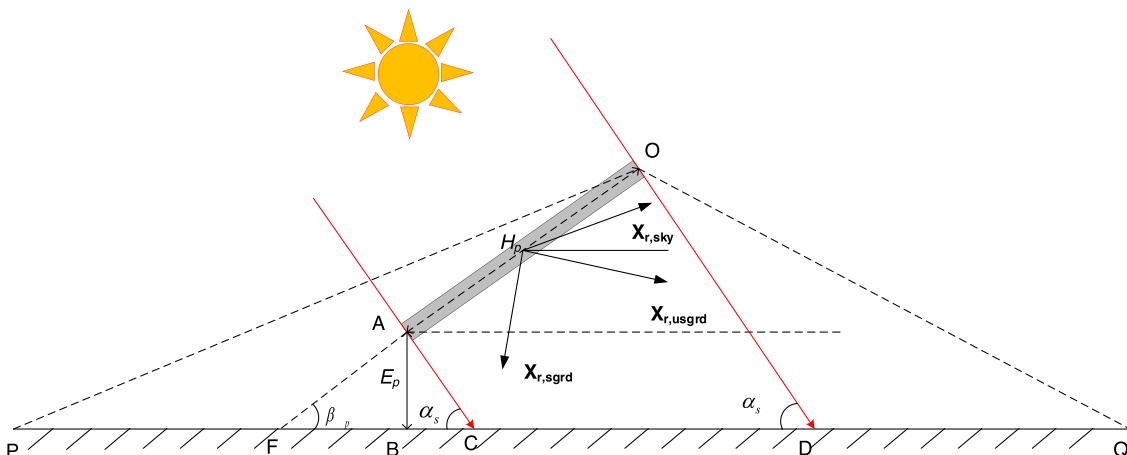


Fig. 10. Schematic diagram of a bPV rear-side view factor [21].

Under the case, the rear-side irradiance can be calculated from Eq. (5):

$$\begin{aligned} G^R &= G_b^R + G_d^R + G_r^R \\ &= (GHI - DHI) \cdot R_b^R + DHI \cdot X_{R,sky} + GHI \cdot \rho_p \cdot X_{R,usgrd} + DHI \cdot \rho_p \cdot X_{R,sgrd} \end{aligned} \quad (5)$$

where the superscript 'R' refers to rear side, R_b^R is the ratio of rear tilted irradiance and horizontal irradiance, $X_{R,sky}$, $X_{R,usgrd}$ and $X_{R,sgrd}$ is the

view factor of rear panel to sky, unshaded ground and shaded ground, respectively. More details can be obtained in the literature [42,43].

(b) Ray tracing model

Besides the view factor model, ray tracing is another approximate tool incorporated in some software, such as RADIANCE [44], packages of Trace Pro [45] and COMSOL [46], to predict the irradiance level of PV panel in a simpler way. After inputting the geometry structure, materials properties, time and location into such software, spectral radiance, irradiance distribution, and glare indices are given as outputs in different forms (color images, numerical values and contour plots). Fig. 11 presents an example about front- and rear-side irradiances at a sunny noontime by RADIANCE software, in which front- and rear-side irradiances reach 844 W/m² and 80–90 W/m², respectively [47].

As for the accuracy, the rear-side irradiance from the view factor model, RADIANCE software and measurement are compared in Fig. 12. It can be clearly seen that the results with the view factor model is in better agreement with the measurements than the RADIANCE software. However, with the help of RADIANCE software, it is capable of obtaining more details than the view factor model, for example the gaps between cell to cell in a module and equipment rack. As a whole, the simulation results of rear irradiance by RADIANCE in the literature are acceptable under most conditions [47], with normalized root mean square deviation (NRMSD) of 4–16% [48].

3.1.2. Electrical model

When it comes to the electrical performance of bPV technology, it is always associated with the relative percentage of bPV and mPV energy

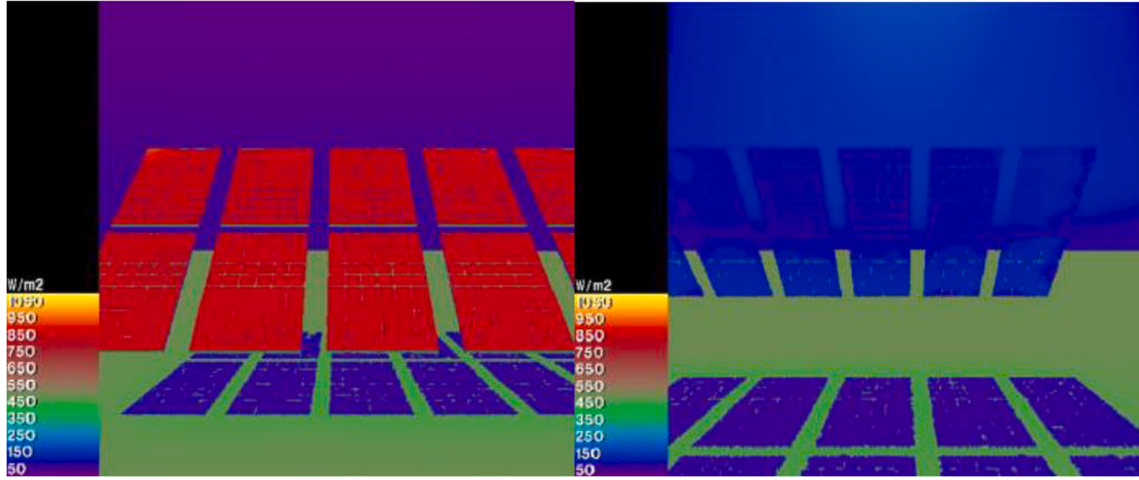


Fig. 11. Front- and rear-side irradiances simulated by RADIANCE [47].

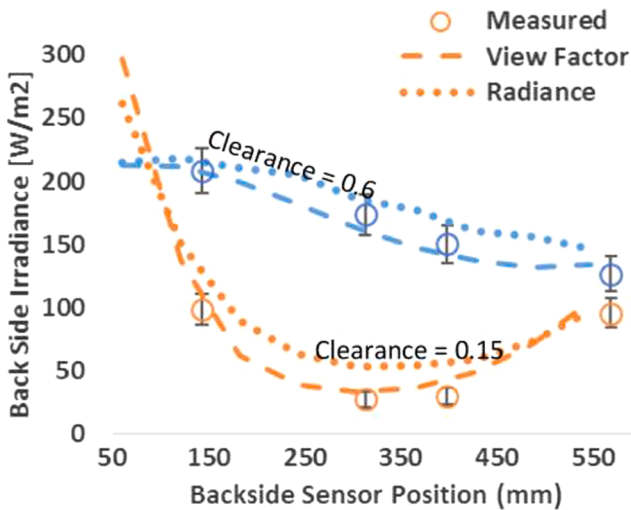


Fig. 12. Comparison of results from view factor model and RADIANCE software [49].

yields under the same conditions, namely bifacial gain to show the advantage of bPV technology, as expressed in Eq. (6) [12,14,50]:

$$\text{Bifacial gain (\%)} = (Y_{\text{bPV}} - Y_{\text{mPV}}) / Y_{\text{mPV}} \times 100 \quad (6)$$

where Y_{bPV} and Y_{mPV} refers to electricity yields of bPV and mPV modules during the test period, respectively.

It can be seen from Eq. (6) that it is rather significant to obtain the value of bPV electricity production for the value of bifacial gain. Therefore, three practical methods, namely a single-point power model, characteristic point model and equivalent circuit model, are introduced in this section to obtain the power output of the bPV modules.

3.1.2.1. A single-point power model. The simplest electrical model is a single-point power model, which is expressed as Eq. (7) [14].

$$P_{\text{PV}} = G^F A \times \eta^F + G^R A \times \eta^R \quad (7)$$

where A is the PV module area, G^F and G^R is front and rear irradiances, respectively, which can be calculated by optical model in 3.1.1.2 or measured by pyranometer, η^F and η^R is the electricity efficiencies of the front and rear PV panels and can be calculated from Eq. (8) and (9), respectively.

$$\eta^F = \eta_{\text{ref}}^F [1 - \beta_{\text{ref}}(T_c - T_{c,\text{ref}})] \quad (8)$$

$$\eta^R = \eta_{\text{ref}}^R [1 - \beta_{\text{ref}}(T_c - T_{c,\text{ref}})] \quad (9)$$

where the subscript 'ref' refers to reference condition, i.e. standard test conditions (STC, solar irradiance $G = 1000 \text{ W/m}^2$, cell temperature $T_c = 25^\circ\text{C}$ and air mass AM = 1.5), β_{ref} is the temperature coefficient of the bPV module, $T_{c,\text{ref}}$ is the cell temperature under standard test conditions (STC), T_c is the cell temperature under non-STC (general operating conditions), η_{ref}^F and η_{ref}^R is the electricity efficiencies of the front and rear PV panel under STC, respectively, which can be calculated from front and rear maximum powers under STC.

3.1.2.2. Characteristic point model. Short circuit current and open circuit voltage are two crucial characteristic points in PV field. Similar to mPV technology, they can be employed to calculate the power output of the bPV module as expressed in Eqs. (10)–(12) [50]:

$$I_{\text{sc}} = I_{\text{sc}}^F + I_{\text{sc}}^R \quad (10)$$

$$V_{\text{oc}} = V_{\text{oc}}^F + (V_{\text{oc}}^R - V_{\text{oc}}^F) \ln((I_{\text{sc}}^R + I_{\text{sc}}^F) / I_{\text{sc}}^F) / \ln(I_{\text{sc}}^R / I_{\text{sc}}^F) \quad (11)$$

$$P_{\text{mpp}} = FFV_{\text{oc}}I_{\text{sc}}(1 + \alpha_{\text{sc}}(T_c - 298.15)) \quad (12)$$

where α_{sc} is the temperature coefficient of the module, P_{mpp} is the power output at maximum power point (MPP) and FF is fill factor.

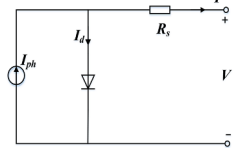
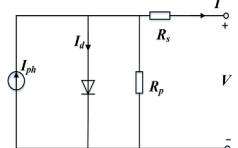
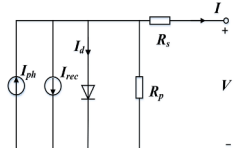
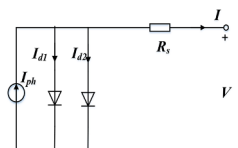
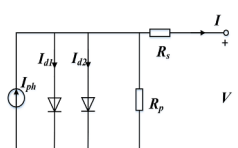
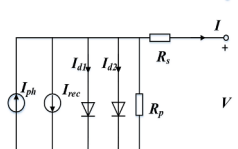
3.1.2.3. Equivalent circuit model. As mentioned above, it is easy to calculate the power output according to the above approaches. However, they can only get some results with low accuracy, thus deterring the popularity of the approaches. Therefore, a highly accurate equivalent circuit model is usually used in academic circles. Table 2 summarizes various equivalent circuit models according to the number of diodes and parameters.

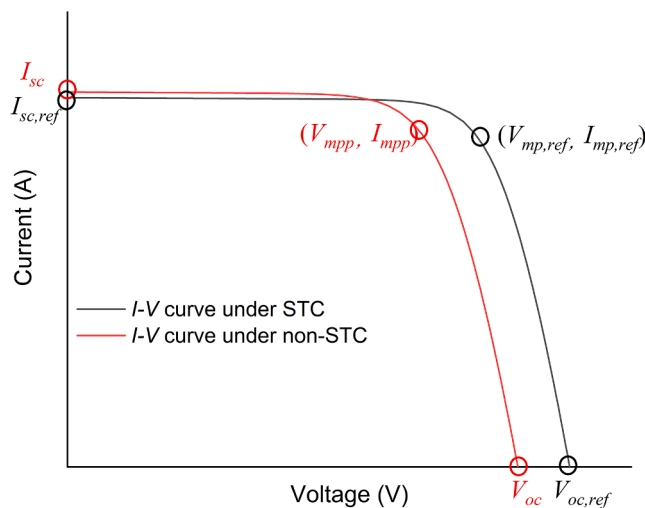
Based on the model listed in Table 2, the characteristic curves of front-side bPV modules under STC can be calculated as shown in Fig. 13. Then, the characteristic curves of bPV modules under non-STC can also be obtained as Eqs. (13)–(19) with the concept of equivalent irradiance [61,62]. The bPV power output can be calculated unless the voltage and current at MPP under non-STC can be obtained.

$$I_{\text{ph}} = \frac{G_E}{G_{\text{ref}}} (I_{\text{ph,ref}} + \alpha_{\text{sc}} \cdot (T_c - T_{c,\text{ref}})) \quad (13)$$

Table 2

Summary of various equivalent circuit models.

| Group | Model | Parameters | References | Equivalent circuit |
|-----------|-------------------|--|---|---|
| One-diode | 4-parameter model | I_{ph} , I_0 , R_s , n | Tossa et al. [51] |  |
| | 5-parameter model | I_{ph} , I_0 , R_s , R_p , n | Mermoud et al. [52]; Gu et al. [21] |  |
| | 6-parameter model | I_{ph} , I_0 , R_s , R_p , n , I_{rec} | Merten et al. [53–55]; Piccoli [56] |  |
| Two-diode | 6-parameter model | I_{ph} , I_{01} , I_{02} , R_s , n_1 , n_2 | Dobos et al. [57]; Tossa et al. [51] |  |
| | 7-parameter model | I_{ph} , I_{01} , I_{02} , R_s , R_p , n_1 , n_2 | Yordanov et al. [58]; Yusufoglu et al. [59] |  |
| | 8-parameter model | I_{ph} , I_{01} , I_{02} , R_s , R_p , n_1 , n_2 , I_{rec} | Merten et al. [60]; Tossa et al. [51] |  |

**Fig. 13.** The characteristic curves and parameters.

$$I_0 = I_{0,ref} \left(\frac{T_c}{T_{c,ref}} \right)^3 \exp \left[\frac{qE_g}{K} \left(\frac{1}{T_{c,ref}} - \frac{1}{T_c} \right) \right] \quad (14)$$

$$R_s = R_{s,ref} \quad (15)$$

$$R_p = \frac{G_{ref}}{G_E} R_{p,ref} \quad (16)$$

$$V_t = \frac{T_c}{T_{c,ref}} V_{t,ref} \quad (17)$$

$$G_E = G^F + G^R \cdot \varphi \quad (18)$$

$$\varphi = \min \left(\frac{I_{sc,ref}^R}{I_{sc,ref}^F}, \frac{P_{max,ref}^R}{P_{max,ref}^F} \right) \quad (19)$$

where E_g is band gap, q is electric charge, K is Boltzmann's constant, G_E is the equivalent irradiance which will be further discussed in Section 3.6.1, φ is the bifacial coefficient [63].

3.1.3. Thermal model

Thermal models include different formulas to estimate the bPV cell temperature. This section discusses these different available models.

3.1.3.1. Sandia model. In Sandia model, the cell temperature can then be obtained when the module temperature is estimated firstly as presented in Eqs. (20) and (21) [64,65]:

$$T_m = G \cdot (e^{S_1 + S_2 \cdot u_w}) + T_a \quad (20)$$

$$T_c = T_m + \frac{G}{G_{ref}} \Delta T \quad (21)$$

where S_1 and S_2 are parameters depending on the module construction and materials as well as on the mounting configuration, G_{ref} is irradiance under STC (1000 W/m^2) and ΔT is a temperature difference parameter, which defines the temperature difference between the module and cell temperatures.

3.1.3.2. NOCT model. Normal operating cell temperature (NOCT) model is employed to calculate the cell temperature of the bPV module by Yusufoglu et al. [59] and Shoukry et al. [50]. In their models, the T_{NOCT} is 2°C higher than that for estimating the mPV cell temperature.

$$T_c = T_a + \frac{T_{NOCT} - 20}{800} G \quad (22)$$

where T_a is the ambient temperature, T_{NOCT} is the nominal operating cell temperature in $^\circ\text{C}$ which is usually provided by the manufacturer for mPV and G is the sum of irradiance on both sides.

3.1.3.3. PVsyst. The performance of bPV modules can be estimated by PVsyst software in newer versions, in which a thermal model based on the Faiman model [66] in Eq. (23) is employed.

$$T_c = T_a + \frac{\alpha G(1 - \eta)}{U_0 + U_1 \times WS} \quad (23)$$

where α and η is the absorptivity and the electrical efficiency of the bPV module, respectively, U_0 is the constant heat transfer coefficient ($25 \text{ W/m}^2\text{K}$) and U_1 is the convective heat transfer component ($1.2 \text{ W/m}^3\text{s K}$).

3.1.3.4. Heat transfer model. To calculate the cell temperature based on energy balance, it is rather necessary to get the energy flows in the bPV system, as presented in Fig. 14. The sunlight is the input. A portion of the sunlight at the front side is absorbed by the glass, while the rest is transmitted and absorbed by the bPV cells. The solar path in the rear-side PV panel is similar to the front side. The bPV cells absorb the sunlight from both sides simultaneously to generate electricity because of the photoelectric effect. Various losses in the cell (transmission losses and thermalization losses) are treated as an internal heat source. The heat is then conducted to the front and rear glasses and is finally dissipated as convective and radiative heat losses.

Once the energy flows in the bPV module are considered accurately, various losses such as radiative losses and convective losses can be calculated [67]. Later the cell temperature of the bPV module can be

obtained according to energy conservation.

3.1.4. Empirical formulae

Besides various models, empirical formulas can also be used to get some quick results, although their accuracy might be compromised.

3.1.4.1. Kutzer model. The effects of albedo, bifaciality, row-to-row distance and height on the additional bifacial energy gain are taken into consideration in the Kutzer model [68] as presented in Eq. (24).

$$BG_E(\%) = \rho_p \times \text{Bifaciality} \times 0.95 \times \left[0.317 \left(1 - \frac{1}{\sqrt{r}} \right) \left(1 - e^{-\frac{8.691h}{r}} \right) + 0.125 \left(1 - \frac{1}{r^4} \right) \right] \quad (24)$$

where BG_E is additional bifacial energy gain, r is the normalized row spacing ($r = R/CW$, where R is the row spacing distance and CW is the PV collector width) and h is the normalized clearance height of the PV panel ($h = H_p/CW$, where H_p is the clearance height of the PV panel).

3.1.4.2. Castillo model. Some experimental tests were performed by Castillo et al. [69], and an empirical best-fit model based on the experimental results is defined to predict annual energy yield of the bPV modules as presented in Eq. (25).

$$BG_E[\%] = 0.317 \times \beta_p [^\circ] + 12.145 \times H_p [\text{m}] + 0.1414 \times \rho_p [\%] \quad (25)$$

where β_p is the tilt angle of the bPV panel tilted at $7.5\text{--}35^\circ$. There are certain limitations to estimate the bPV performance using this empirical model under some complex conditions instead of theoretical analysis.

It can be observed from Eqs. (24) and (25) that BG_E is always proportional to H_p in the Castillo model. The growth rate reduces as H_p increases in the Kutzer model, although BG_E increase with a rise of H_p in these two models. In all, these empirical formulas are only used to get some rough results to guide the design of a bPV system, and cannot replace a coupled model to estimate the bPV performance with high accuracy.

3.2. Software simulation of bPV

The performance of bPV especially electrical performance, can be obtained accurately from coupled models described above, although it is complicated and unnecessary for some beginners to understand these relationships. Under such circumstances, simulation software may be a good choice because of their simplification, such as bifacialvf [70], PV_Lib Toolbox [71], System advisor model (SAM) [72] and PVsyst software [73]. In this section, SAM and PVsyst is introduced briefly as a representative of open source software and commercial software, respectively.

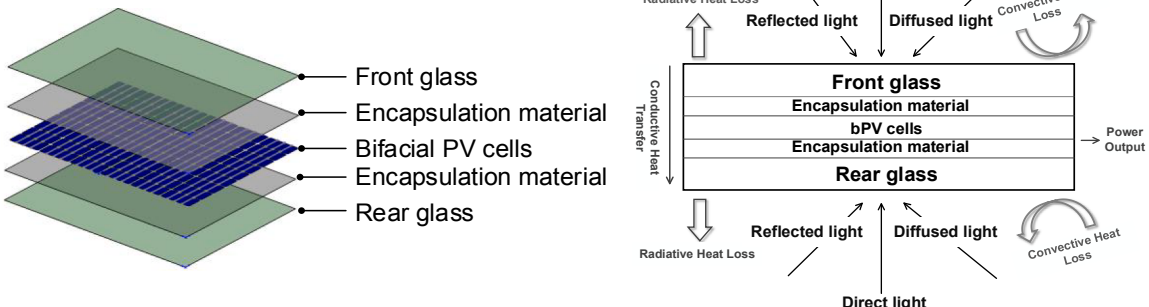


Fig. 14. Structure and energy flows for the bPV module.

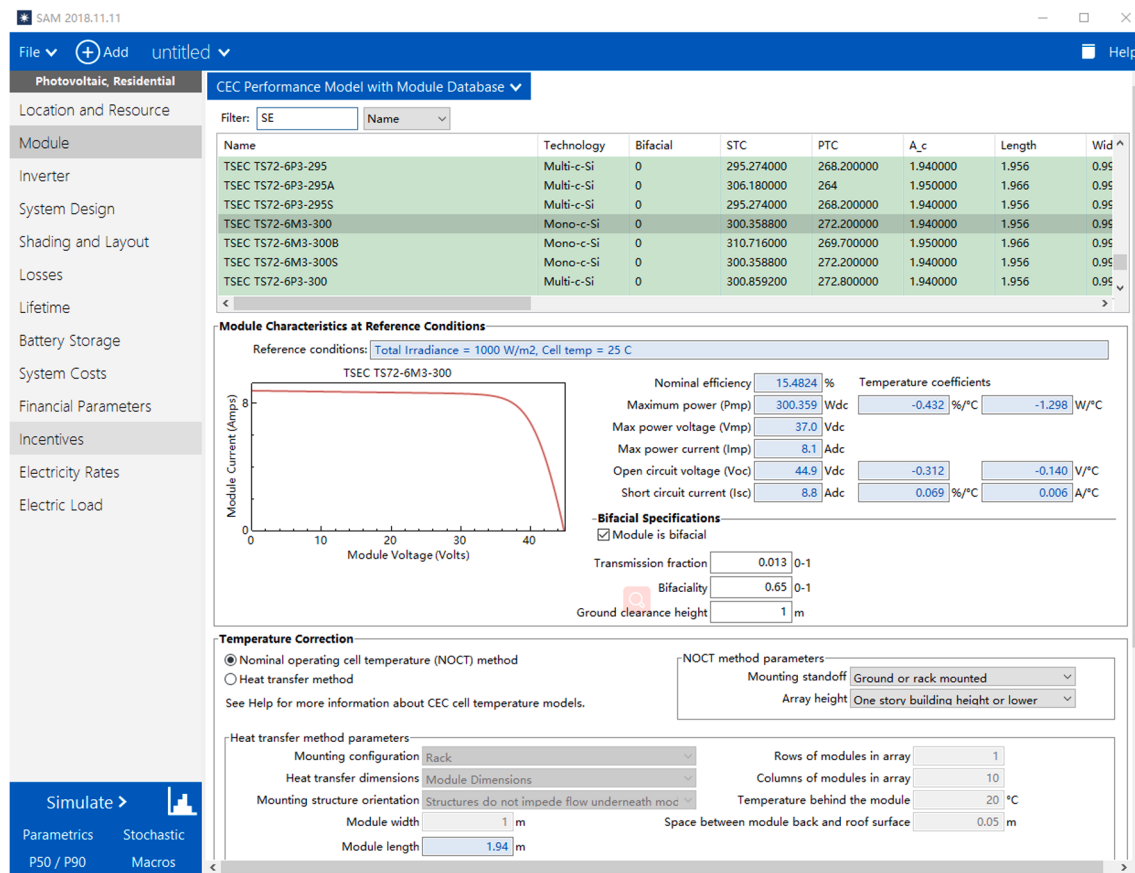


Fig. 15. Software interface of bifacial system design for SAM [72].

3.2.1. SAM

SAM is also developed by the National Renewable Energy Laboratory (NREL) to model techno-economic performance of various renewable energy systems, including bPV systems [72]. Fig. 15 presents the interface of SAM for bifacial system design. It can be observed that bPV performance is based on the characteristic parameters of the front side at reference conditions. Bifacial specifications, namely transmission fraction, bifaciality, and ground clearance height are the variables to be determined by designers. It should be noted that two methods are selective to make temperature corrections, namely NOCT method and heat transfer method as aforementioned.

3.2.2. PVsyst

PVsyst software is widely-used for designers in the PV simulation field. A bifacial model is also introduced into this typical software under some assumptions. The main assumptions include having an equal row distance and a very long PV string without considering edge effects. Two bifacial models are provided to estimate the bPV performance, including unlimited sheds 2D-model and unlimited trackers 2D-model, as presented in Fig. 16. The difference between these two bifacial models is that the former is for fixed bPV arrays while the latter is for horizontal single-axis tracking bPV arrays.

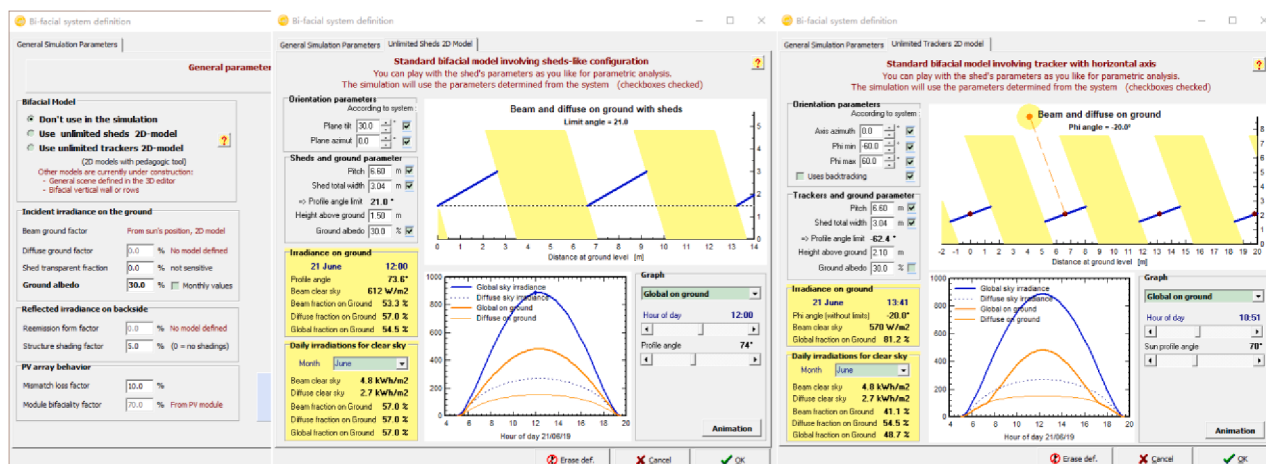


Fig. 16. Software interface of bifacial system design for PVsyst [73].

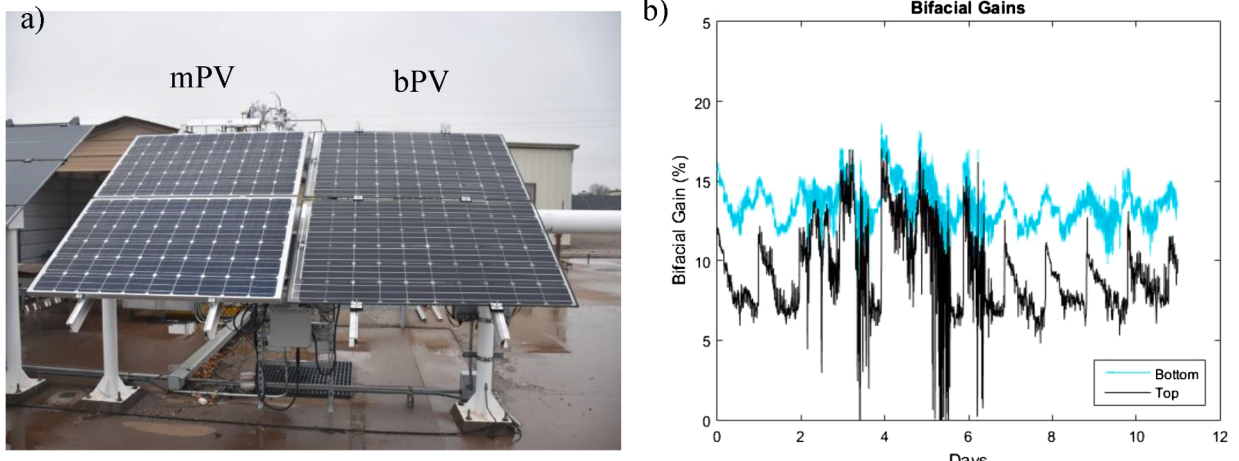


Fig. 17. A field example of bPV performance by Sandia National Laboratories: a) experimental set-up; b) bifacial gain as experimental results [74].

3.3. Experimental study and real system operation performance

Besides numerical simulations, some experiments were carried out not only to validate models, but also obtain the performance of bPV modules under real operation conditions.

In a field example [74], two mPV and two bPV modules facing south were installed at a tilt angle of 35° (Fig. 17 (a)), and bifacial gains of the top and bottom rows were calculated. Bifacial gains of the two rows fluctuated from about 7% to 16% (Fig. 17(b)). The bifacial gain of the bottom row was higher than that of the top row because of the short distance from the bright area for the bottom modules. For one clear day, the bifacial gain was still fluctuating and the value in the morning was the highest of the whole day due to the relative position of these two modules: the sunlight in the morning hits the ground directly beneath the bPV module while the shadow was projected under the mPV module.

Similar experiments for estimating the bPV performance were also conducted by other research groups. For example, the annual bifacial gain reached 5% at south orientation, with 40° tilt angle and an albedo of 0.05 [75]. Many factors influence the bifacial gain. For exploring the effects of various factors, 7 different test conditions were employed by Castillo et al. [69] to calculate the annual average bifacial gain in field,

varying from 12.3% to 30% and a best-fit relationship between bifacial gain and various factors was developed. Bifacial gains of different background were measured by experiments: 7.6% on grass, 15% on sand and 29.2% on snow [19]. To obtain higher bifacial gains, some optimized system designs by experiments were proposed, such as higher albedo, fewer backside obstructions and less ground shading beneath the array [18]. Through experiments, Rabanal-Arabach et al. [76] found that albedo and ambient temperature were the main module temperature drivers. Reduction of infrared reflection and increasing visible wavelength reflection were suggested to improve the bPV performance and reliability, especially in desert areas. Some experiments validated that micro inverter is much more proper than string inverter, with a higher index of bifacial gain [17,18].

3.4. Economic issues of bPV

The bPV modules are highly recommended in PV market, especially some developed countries with high labor cost, because of the lower price for balance of system and operation expense [38,77]. Therefore, LCOE is a significant concept in PV economic estimation, as it reveals if the grid parity of electricity produced by PV can be realized [38], and is

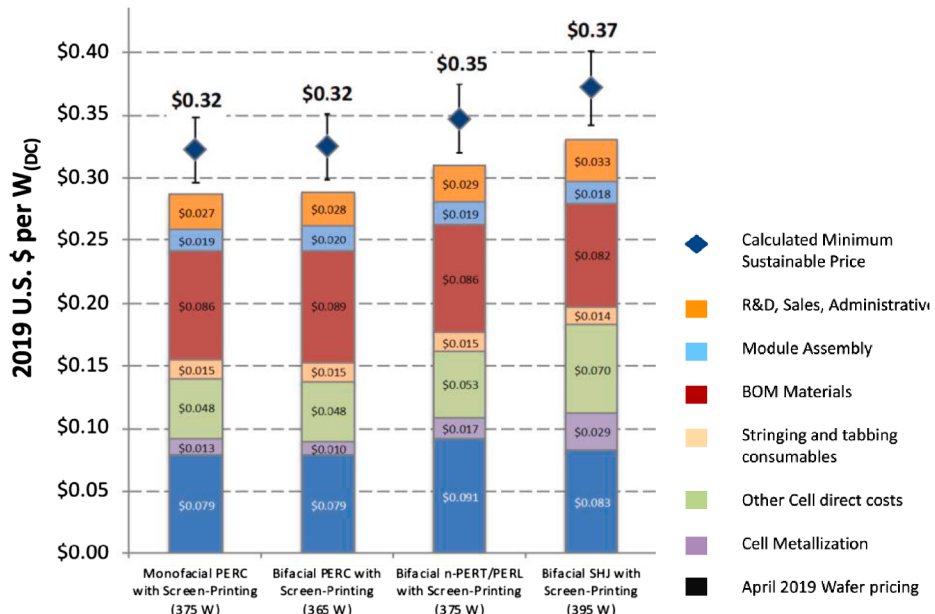


Fig. 18. Manufacture cost of mPV and various bPV modules [79].

defined as [78]:

$$LCOE = \frac{\sum_{n=1}^N \frac{C_n}{(1+r_{dr})^n}}{\sum_{n=1}^N \frac{E_n}{(1+r_{dr})^n}} = \frac{\sum_{n=1}^N \frac{I_n + O_n + M_n + F_n}{(1+r_{dr})^n}}{\sum_{n=1}^N \frac{S_n (1-d)^n}{(1+r_{dr})^n}}$$

where N is the lifetime of a PV project, r_{dr} is discount rate, d is degradation rate, E_n and S_n are actual and rated electricity production in year n , and net costs C_n in year n contains initial investment I_n , operation costs O_n , maintenance costs M_n and interest expenditures F_n .

It is well acknowledged that the differences of LCOE between bPV and mPV are mainly associated with two factors, namely energy production and initial cost especially the cost of manufacturing. Energy production of mPV and bPV is affected by various other factors and will be discussed in Section 3.5. The mPV and bPV manufacturing cost is demonstrated in Fig. 18. It can be seen that the difference in manufacturing cost between various bPV technology and mPV reaches 0–15.6% depending on manufacturing technology. It is noted that the cost of bifacial PERC technology is the same as mPV. The manufacture cost will reduce constantly as bPV technology develops further, ultimately reducing the LCOE.

The research on economic issues of bPV, especially LCOE will be a hot topic in the future, although there are just a few studies on LCOE of bPV as of now. It is well known that the use of bifacial technology on PV cells can contribute to lower the LCOE than conventional mPV cells in real applications, [80], up to 2–6% [15], but the value of LCOE is in fact affected by various factors such as installation and location. Tillmann et al. [81] obtained a function of minimum LCOE with row distance and tilted angle for various land consumption costs based on Bayesian optimization algorithm, which can offer some suggestions on the reduction of LCOE up to 23%. Range of LCOE around the world is from 3.29 to 14.43 cents/kWh, which mainly depends on the ground albedo and solar irradiance. The specific value of LCOE for numerous cities can be found in Ref. [16]. The concept of LCOE can also be employed to determine which one is more cost-effective for mPV and bPV modules with any module orientation (AMO) or vertical module orientation (VMO). The results obtained by Rodríguez-Gallegos et al. [16] from global perspective show that for latitudes higher than 40°, bifacial AMO modules are always more cost-effective than mono-facial AMO systems regardless of ground albedo. However, this trend is reversed for latitudes

below 40° unless the albedo value is higher than a minimum value of about 0.12–0.30. For the comparison between mono-facial AMO and bifacial VMO, the latter is more cost-effective under two conditions: 1) latitudes are higher than 65°; 2) the albedo is higher than a minimum value of 0.29–0.57, although latitudes are below 65°.

3.5. Various impact factors of bPV module performance

As Fig. 19 shows, the bPV performance is governed by various factors including three aspects. These include bifacial technology, local meteorological and geographical information (sun position, soiling, shading, diffuse coefficient and ground albedo) and installation information (orientation, tilt angle, row distance and module elevation) [82]. In this section, some important factors will be discussed in detail.

3.5.1. Albedo

Rear irradiance is largely dependent on the reflection of the ground. High albedo contributes to high rear irradiance, resulting in high bifacial energy yield [83]. Therefore, the bifacial gain also has a linear growth relationship under almost constant front irradiance when albedo increases [21,59], implying that the bPV technology can take full advantage to generate more electricity in some places of high albedo [84]. For example, the bifacial gain can reach 7.6%, 15.4% and 29.2% for ground having grass, sand and snow, respectively [19].

3.5.2. Tilt angle

Besides albedo, tilt angle also affects bPV performance greatly. The annual energy generation of the bPV and mPV modules increases slightly until their optimal angles are reached and then decreases sharply. It is noted that the optimal angle of bPV modules is higher than for mPV under the same conditions [14,15]. Tilt angle has less effect on the rear-side energy yield compared to the front-side. This is due to negligible effects on the diffuse and reflected irradiances from the sky and ground, demonstrating total bifacial energy yield and corresponding continuous increase in bifacial gain. High bifacial gain for a large tilt angle can explain well the fact that vertical bPV technology is more recommended in some scenarios, such as for the facade of a building and for noise barriers.

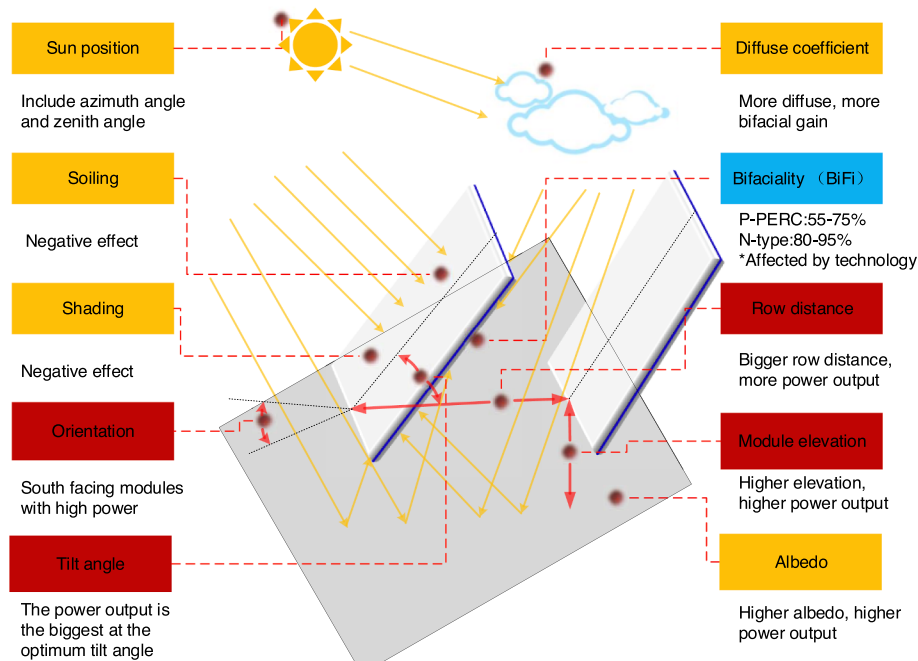


Fig. 19. Various factors affecting the performance of the bPV modules.

3.5.3. Elevation

Elevation also affects the bifacial energy yield by affecting the rear irradiance [59]. Due to more reflected irradiance from the ground and less self-shading, bifacial energy yield and bifacial gain accelerate at high elevation, but with a small growth rate [47,85]. Therefore, it is usually suggested to set the elevation of the bPV modules as 0.5–1.5 m above ground level, to comprise electrical gain with the size of space [21,59].

3.5.4. Orientation

Bifacial PV performance greatly varies with the orientation as it affects the received irradiance [86]. Fixed and tracking cases are considered, in order to accurately evaluate the effect of orientation. Both bPV and mPV modules with tracking technology produce more electricity than the fixed modules because of more irradiance. However, tracking technology does better to front-side irradiance than the rear-side, resulting in lower bifacial gain with a tracking system. For the fixed case, the modules are installed facing south for higher energy yield. When facing east or west, the modules produce a little lower energy yield, but with higher bifacial gain, indicating that bPV technology is more flexible compared with the mPV, without the limits of orientation. It is noted that the bPV power curve has two peaks when the bPV module is vertical and east–west-facing, while the mPV module has one peak power point, as presented in Fig. 20 [14].

3.5.5. Row distance and row number

For more electricity production, many bPV modules are connected in series and parallels to form a bPV array. Under the circumstance, field installation (row distance and row number) becomes an indispensable factor of affecting the bPV performance [49,87]. According to the study of Shoukry et al. [50], bPV performance is better with larger row spacing. When the distance between the module rows is fixed at 2.5 m, the bifacial gain for the PV modules in a PV array with 5 × 11 modules is presented in Fig. 21 [50]. The performances of the modules at the edge and at the center of the field vary from 31.41% to 27.72%, which are obviously lower than a stand-alone bifacial module (33.85%).

3.5.6. Soiling and shading

It is obvious that soiling and shading have a negative effect on bifacial performance. To estimate the negative effect of soiling, the concepts of soiling loss in energy generation and soiling rate were employed by Bhaduri et al. [32] and Luque et al. [88]. Results show that vertical bPV modules have less soiling loss and average soiling rate. In addition, soiling loss of the bPV module is much lower than that of mPV, both for front and rear sides. Furthermore, a cleaning optimization model was developed to guide the cleaning strategy, suggesting that there is no need to clean the rear side because of less than 3% difference for cleaning as compared to not cleaning the rear-side.

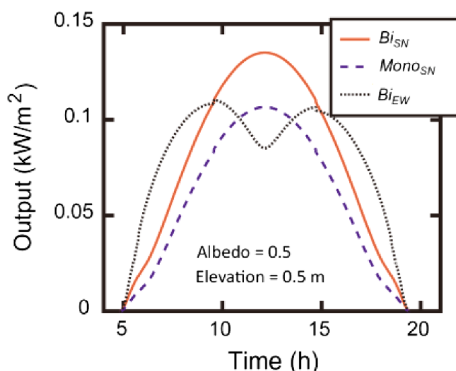


Fig. 20. PV power output with different orientations (Mono_{SN} : south–north-facing mPV at optimal tilt angle; Bi_{SN} : south–north-facing bPV at optimal tilt angle; Bi_{EW} : vertical east–west-facing bPV) [14].

For the shading effect, the bPV modules were validated by experiment to have 12.74% lower shading power loss rate than the mPV by affecting the fill factor [89,90]. Moreover, the further behind the module and the whiter the shading objects are, the lower the loss of the bPV system becomes [91], which suggests that it is better to place the white rocks further behind the PV module if it cannot be avoided.

In all, bPV technology has an advantage of suffering from less power loss due to soiling and shading under the same weather and installation conditions.

3.6. Test and characterization of the bPV modules

A standard test and characterization method is vital for bPV technology, which can provide manufacturers from different regions with a common approach to examine the bPV performance. Usually these test methods can be divided into two categories, namely indoor and outdoor.

3.6.1. Indoor performance characterization

As for bPV indoor performance characterization, it can be classified into single-side illumination and double-side illumination according to the number of light sources. For single-side illumination, front- and rear-side PV panels are tested under 1000 W/m^2 separately, when the light from the opposite side is eliminated with a black rear cover placing at a distance from the PV panel as presented in Fig. 22(a1)–(a3). Then, the power output can be regarded as an expression of equivalent irradiance, which is also adopted in a technical specification, namely IEC TS 60904-1-2, published in 2019 [92].

For the equivalent irradiance, it can be expressed as Eq. (27):

$$G_{\text{Ei}} = G^{\text{F}} + \varphi G_i^{\text{R}} \quad (27)$$

where G_{Ei} is the equivalent irradiance of the bPV modules, and φ is the bifaciality, the minimum value between the bifaciality coefficients of short-circuit current and maximum power under STC.

Therefore, two specific values of bPV power output, P_{maxBG_E100} and P_{maxBG_E200} , can be calculated as Eq.(28) and (29) under two reference irradiances ($G_{\text{R1}} = 100 \text{ W/m}^2$, $G_{\text{R2}} = 200 \text{ W/m}^2$):

$$P_{\text{maxBG}_E100} = P_{\text{max,ref}} + BG_E \cdot 100 \quad (28)$$

$$P_{\text{maxBG}_E200} = P_{\text{max,ref}} + BG_E \cdot 200 \quad (29)$$

Another approach is double-side illumination based on the simultaneous illuminations of both sides with front irradiance at 1000 W/m^2 and at least two different rear irradiance. Apparently it is more straight but time-saving compared with single-side illumination, and different setups are employed during the testing process, such as two solar simulators (Fig. 22b), tilted mirrors [35] (Fig. 22c), and a well-defined reflector (Fig. 22d), which also introduces some problems and challenges during the testing period [93]. For two solar simulators, timing the two flashes simultaneously and controlling the reflected irradiance from the surroundings at the expense of additional solar simulator should be taken into consideration. For the tilted mirror, only several rear-side irradiances can be set by a filter instead of a continuous irradiance level. For the well-defined reflector, there are also many problems such as non-uniform rear irradiance, setting up specifications of the reflector material and distance from the bPV module [87].

3.6.2. Outdoor performance characterization

Similarly, it can also be classified into single-side illumination and double-side illumination for outdoor performance characterization of the bPV module. For single-side illumination, the concept of equivalent irradiance in Section 3.6.1 is still valid during the tests as presented in Fig. 23(a) where sunlight is the source of the outdoor experiment. For double-side illumination, a reflective cloth or surfaces with a distance of 0.5–1 m from the bPV panel bottom are employed in order to change the ground albedo. At least two specific power values with different rear

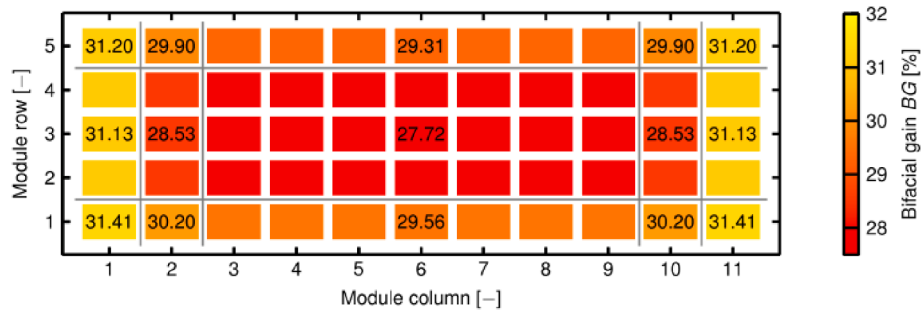


Fig. 21. Bifacial gain for a PV array with many rows [50].

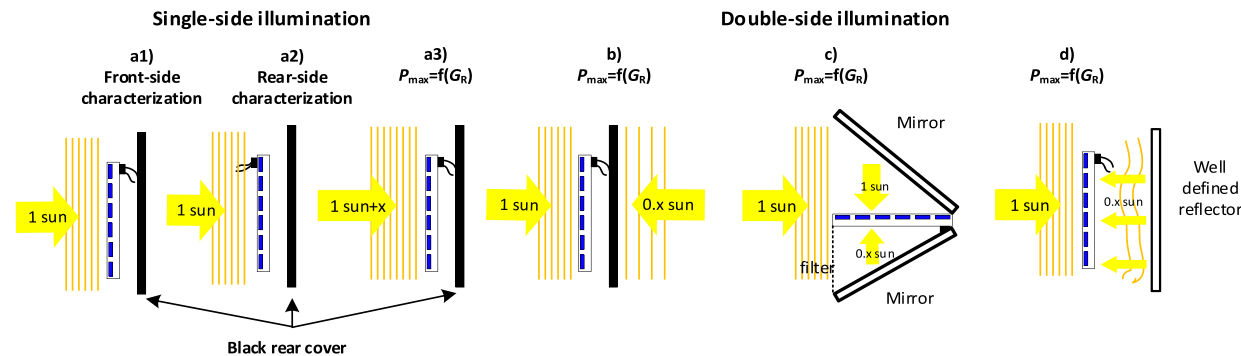


Fig. 22. Schematic measurement of indoor performance characterization: single-side illumination (a1, a2 and a3); double-side illumination (b, c and d) [87].

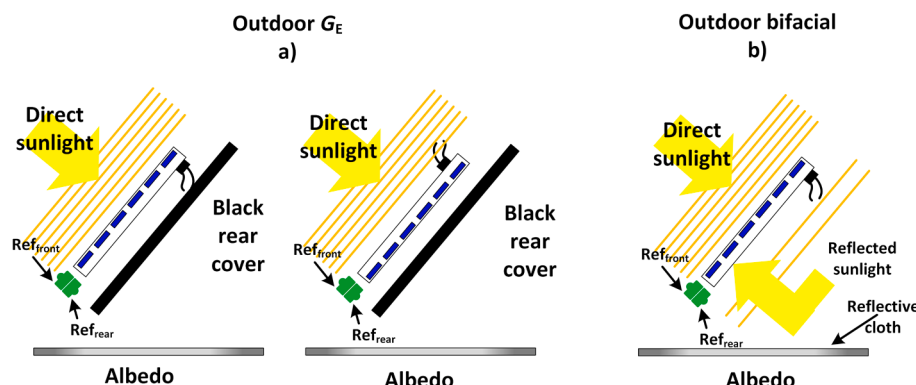


Fig. 23. Schematic measurement of outdoor performance characterization: a) single-side illumination; b) double-side illumination [87].

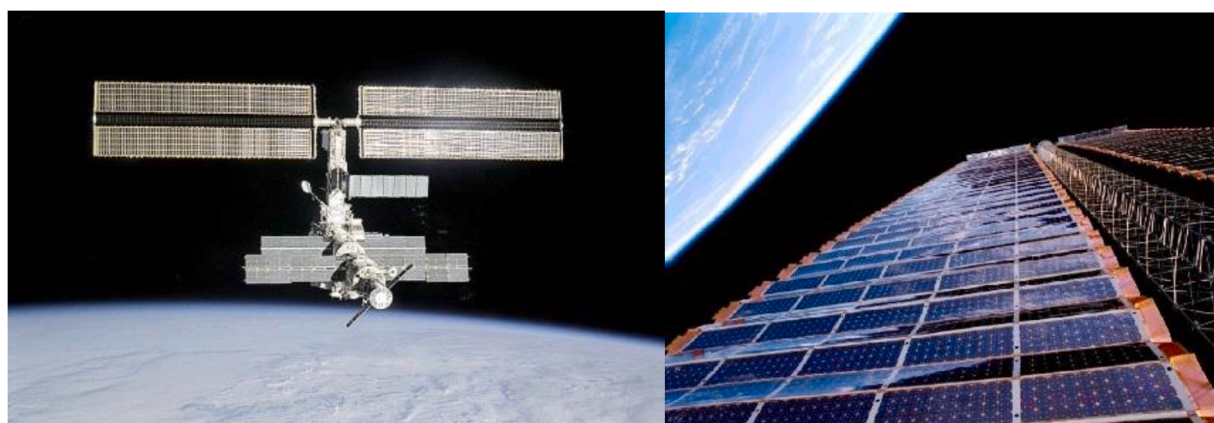


Fig. 24. The bPV modules on International Space Station [97].

irradiances are also provided in Eq. (28) and (29). More details can also be found in the technical specification IEC TS 60904-1-2 [92].

3.7. Practical applications

The bPV development can also be useful in many applications, including both space and terrestrial applications.

3.7.1. Space applications

The first space applications of bPV technology in the world could date from a space station named Salut-3 in 1974 [94]. Bifacial n⁺-p-p⁺ contributed to a giant increase in electricity production, up to 34%, which led to the installation of bPV arrays on Salut-5 space station launched in 1976 [95]. Later, bPV arrays were installed on some satellites and famous spacecrafts [96], especially the bPV arrays on International Space Station (ISS), which consists of two American bPV arrays (December 2000), Russian "Zarya" (November 1998) and "Zvezda" (July 2000) Solar Arrays as presented in Fig. 24.

3.7.2. Terrestrial applications

3.7.2.1. Large-scale bPV plants. As lower LCOE is preferred by the PV market, the utilization of sunlight from both sides contributes to the development large-scale bPV plants. In 2013, the world's first large-scale bPV power station with an installed capacity of 1.25 MW_p was set up in Hokuto City, Japan [98]. The PV plant showed huge electrical benefits and thus strengthened the confidence of investors, persuading them to install more bPV plants around the world. Therefore, more and more large-scale PV plants with bPV technology were set up, as presented in Table 3.

3.7.2.2. Building integrated with bPV. Besides the bPV plants, bPV technology is also employed into building integrated photovoltaics (BIPV) [106], such as vertical facade integration [35], shades [107] and fences [108] (see Fig. 25). There are numerous advantages to this application. Firstly, they not only generate electricity, but also function like conventional building materials. In addition, they remain clean and thus huge cleaning costs can be reduced as they are less sensitive to snow, dust, etc. Moreover, the orientation effect is not as strong as for conventional mPV modules, meaning that they can face any orientation, including east and west, which was unimaginable in the past [109].

3.7.2.3. Noise barriers. With increasing population and land price, there is not enough potential for PV installation within cities. Under such conditions, vertical noise barriers (Fig. 26) are considered as an ideal

solution to facilitate economy development and renewable energy supply [34]. Therefore, the first PV noise barriers were built in 1989 in Chur, Switzerland [111], in which mPV modules were employed, followed by some other pilot installations [34]. In 1997, the first bPV noise barriers in the world were installed and put into use in Switzerland [110]. After these initial attempts, noise barriers with bigger capacities were built, for example, a bPV noise barrier of 730 kW_p was installed in Italy in 2009, and a series of bPV noise barriers ranging from 1 MW_p to 2.065 MW_p were installed in Germany [34].

3.8. Summary of bPV and mPV technologies

As described above, bPV technology has its own characterizations. Therefore, it is necessary to compare bPV and mPV from many perspectives, such as cell structure, power generation and applications as summarized in Table 4.

4. Outlook of bPV technology

As mentioned above, a lot of work has been done on bPV development in areas of modelling, experiments, and potential applications. However, there are still some challenges of modelling and performance estimations, which still require more research to move ahead. Therefore, in this section an outlook of the bPV technology is presented with some challenges and perspectives for future development.

4.1. Challenges of bPV technology

As the market of bPV technology increases rapidly, corresponding challenges have gradually emerged out, which hinder its widespread development.

4.1.1. Electrical mismatch

Electrical mismatch of bPV cells may be regarded as the biggest challenge by most people, which mainly result from uneven rear irradiance, as presented in Fig. 27 [91]. The highest rear irradiance of the PV cell (83 W/m²) is 177% of the lowest rear irradiance (47 W/m²). Such irradiance differences could result in uncertainty and reduction in power output by affecting the fill factor [85,93]. When these modules with inhomogeneous irradiance are connected in series and parallels to form a large-scale PV array, mismatch loss will contribute a great proportion in the whole system loss and thus need to be carefully controlled [87,112]. Therefore, the non-uniformity of less than 3 W/m² rear irradiance is highlighted several times in the technical specification IEC TS 60904-1-2 [92], which gradually becomes a huge challenge to face and solve in the PV field [89]. Therefore, despite various irradiance models being proposed, a suitable simplified and accurate model is lacking, especially for rear-side irradiance, which thus requires further research.

4.1.2. Systems optimization

Besides various losses in bPV cell and from cell to module as described in Section 2.4, components including inverters, MPPT and others should also be taken into consideration from manufacturing to installation to reduce the related energy losses for a specific bPV system as presented in Fig. 28 [6]. DC wiring loss, DC-DC conversion, DC-AC inversion, AC wiring loss and transformer loss are some examples, which were rarely discussed in the past but should be paid more attention in the future.

4.1.3. Performance estimations

Unlike conventional energy sources, multi-physics processes are involved in bPV power generation. These include optical, electrical and thermal processes, which are tightly coupled, but rarely discussed in literature with relation to sunlight, electricity and heat. In addition, power output from the bPV modules is always represented as a linear relation of front-side power under STC, and several particular rear-side

Table 3
Summary of global large-scale bPV plants [98–105].

| Time | Location | Installed capacity (MW _p) | Module type, Manufacturer |
|------|---|---------------------------------------|--|
| 2013 | Hokuto City, Japan | 1.25 | EarthON 60 (EarthON cell), PVG Solutions |
| 2015 | Valparaiso, Chile | 2.50 | n-type BiSoN module (BiSoN cell), Megacell |
| 2016 | Datong City, Shanxi Province, China | 50 | n-type Panda module, Yingli Solar |
| 2017 | Wuhai City, Inner Mongolia Autonomous Region, China | 100 | n-type Panda module, Yingli Solar |
| 2018 | Dongying City, Shandong Province, China | 100 | PERC module, Almaden |
| 2019 | Netherlands | 11.75 | p-type module, Jolywood Solar |
| 2019 | Michel County, Georgia, USA | 224 | PERC module, LONGi Solar |
| 2019 | Traxscara, Mexico | 220 | p-type PERC, LONGi Solar |



Fig. 25. The applications of bPV modules in BIPV.



Fig. 26. Applications of vertical bPV modules as noise barriers [110].

Table 4
Comparisons between bPV and mPV.

| Item | bPV | mPV |
|---------------------|---|---|
| Cell structure | Made of two contacts (front and back), emitter, base, and two layers of anti-reflection coating (front and back) | Made of one front contact, emitter, base, and one front layer of anti-reflection coating and back surface field |
| Cell appearance | The rear side is similar to the front one. | The rear side is very different from the front side mainly due to the back surface field |
| Backsheet materials | Made mostly of glass with transparent, organic backsheet | Made of TPT, TPE, BBF etc. |
| Power generation | Power driven by front and rear irradiances | Power only driven by front irradiance |
| Advantages | <ul style="list-style-type: none"> • Flexible installation • 5–30% more power output • 2–6% lower LCOE • Low cleaning frequency | <ul style="list-style-type: none"> • Convenient installation • Low cost of each PV cell due to mature manufacturing process |
| Disadvantages | <ul style="list-style-type: none"> • Critical installation condition for avoiding shading of the back side • Complex manufacturing process | <ul style="list-style-type: none"> • Affected by weather conditions much • High LCO because of electrical performance • High cleaning frequency • PV plants • BIPV, mostly on the roof |
| Applications | <ul style="list-style-type: none"> • Wide applications, space station, power plant, BIPV (vertical facade integration, shades and fences) and noise barriers | |
| Suggestions | Installation in a tracking system at an optimal tilt angle with high albedo, elevation and row space | Installation in a tracking system or facing south at an optimal tilt angle |

| | A | B | C | D | E | F |
|----|----|----|----|----|----|----|
| 1 | 65 | 64 | 63 | 63 | 63 | 62 |
| 2 | 75 | 74 | 73 | 74 | 75 | 77 |
| 3 | 72 | 70 | 69 | 69 | 68 | 72 |
| 4 | 66 | 65 | 65 | 66 | 68 | 70 |
| 5 | 53 | 50 | 47 | 49 | 52 | 57 |
| 6 | 54 | 51 | 49 | 51 | 52 | 56 |
| 7 | 53 | 54 | 55 | 56 | 58 | 61 |
| 8 | 62 | 59 | 56 | 58 | 59 | 63 |
| 9 | 66 | 61 | 56 | 59 | 61 | 66 |
| 10 | 72 | 67 | 62 | 65 | 69 | 75 |
| 11 | 79 | 78 | 76 | 77 | 78 | 79 |
| 12 | 76 | 73 | 70 | 73 | 77 | 83 |

Fig. 27. Measured rear-side irradiance of each cell in a bPV module [91].

irradiances from manufacturers [21]. However, there is no linear relationship between bPV module power and irradiance, resulting in huge inaccuracy during power estimation, which should be carefully considered. Besides, electrical and thermal performance are always expressed by a simple equation, which cannot express the relationship between them. In fact, temperature distribution and power output are a function of environmental conditions (ambient temperature, wind velocity, solar radiation, and reflected radiation from ground). Moreover, solar irradiance, especially reflected irradiance from ground, is always associated with various installation conditions. Therefore, it is

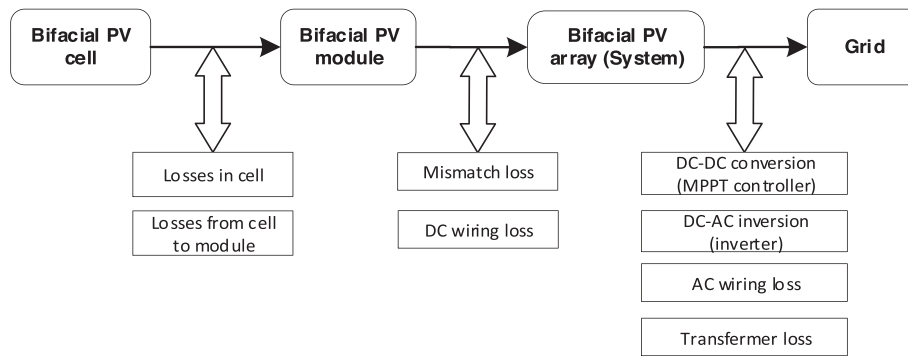


Fig. 28. Various system loss sources for a bifacial system [6].

significant in the future to understand the relationships among them and then model their performance considering both simplification and accuracy.

Apart from modelling, long-term experiments should be conducted to evaluate the power output of bPV modules under real operating conditions, instead of ideal conditions, which may strongly affect the bPV performance.

4.1.4. Economic and environmental estimations

The electrical performance of bPV modules has been discussed by many researchers. In contrast, there are few issues on economic and environmental estimations of bPV modules due to various reasons. On one hand, the value of electricity production is the foundation of the issues on economic and environmental estimations. However, there are still fierce arguments on how to calculate the power output of bPV modules, especially the power from the rear side. On the other hand, economic and environmental estimates, especially LCOE, are rather complicated, because various factors also need to be taken into consideration in the financial model, such as the investment and maintenance costs.

4.2. Potential approaches and perspectives

The above challenges indicate that great efforts are needed to promote bPV technology. In this section, some potential approaches to optimize the bPV technology are discussed from the perspectives of cell, module and system, followed by some future perspectives.

4.2.1. Cost-effective cell designs

Cost-effective cell designs are crucial for better efficiency as presented in Table 5

As the demand of cost-effective bPV modules increases, these novel

Table 5
Cost-effective cell designs.

| No. | Technology | Advantages |
|-----|--------------------------|--|
| 1 | Larger cells | <ul style="list-style-type: none"> Manufacturing cost Reduction Cost reduction on balance of system |
| 2 | Half-cut cell technology | <ul style="list-style-type: none"> Power output improvement by 2%-4% Excellent anti-blocking performance Flexible installation, such as installation on roofs |
| 3 | Multi-busbar technology | <ul style="list-style-type: none"> Splendid appearance [113] Manufacturing cost reduction by saving over 50% silver paste Power increment through strong current collectivity and greater light receiving area small power loss rate even cracked or chipped |
| 4 | Shingling technology | <ul style="list-style-type: none"> Up to 8-9.6% more power [114] Low ohmic loss [114] Low residual cell stress and bowing [115,116] Splendid aesthetics without visible busbars and ribbon soldering [117] |

cell designs combined with bPV technology will be used at a large scale in the near future although more research needs to be done in order to optimize these novel technologies, since they consists of issues like undeveloped equipment, low module yield, high cost, and patent breakthrough.

4.2.2. Up conversion and down conversion

Novel methods with some specific structure to exceed the Shockley-Quisser limit for PV development are proposed, namely up conversion (UC) and down conversion (DC) [118]. Encapsulation structure of a bPV cell with UC is presented in Fig. 29 [119]. UCs in silicone are attached to the back side of the industrial bPV cell. UC is a method of transmitting high-wavelengths (low-energy) photons from the solar spectrum to lower-wavelengths (high-energy) photons [120]. Besides, PbS quantum dots (QDs) are employed in this study at the back side of the UCs layer due to their appropriate properties of absorption and emission. With the structure of UC and QDs, the absorption and efficiency are improved by reducing the reflection and transmittance as presented in Fig. 30. DC occurs when a specific material is used to absorb the photon at short wavelengths and emit it at long wavelengths. The material is always placed on the front side to reduce thermalization loss [121]. In all, UC and DC can be applied in bPV technology in the future to reduce transmission loss and thermalization loss for better efficiency of bPV modules.

4.2.3. Thermal management of bPV

High cell temperature also has negative effect on the performance of bifacial modules [26], the thermal management of bPV modules is a crucial aspect in the future. Photovoltaic/thermal (PV/T) technology has the potential to spread from mPVs to bPVs, but this is met with some challenges, such as designing of the collector in a way that does not affect the irradiance of both sides. Fig. 31 presents two designs of bPV/T, namely air-cooling and water-cooling. Four structures of air cooling are designed by Ooshaksarai et al. [122], in which the energy efficiency of structure two is highest, followed by structure three, four, and one accordingly. For water cooling, 40% bifacial gain of bPV/T is achievable [123]. However, these complex designs cannot obtain such obvious results, and even harm the electricity production due to lower received irradiance. Therefore, further in-depth analysis on novel methods or materials, such as specific selective coolant and coating should be performed in the future for the development of bPV thermal management.

4.2.4. Solar tracking technology

As indicated above, different azimuthal angle means different irradiance on the plane of array due to changeable solar trace, which implies the potential of solar tracking technology combining with bPV technology [124]. Obviously, these solar tracking systems have made use of the well-developed mPV technology in the past decade, especially various intelligent techniques (fuzzy logical, genetic algorithm etc.), while hardly making use of bPV technology. However, tracking systems

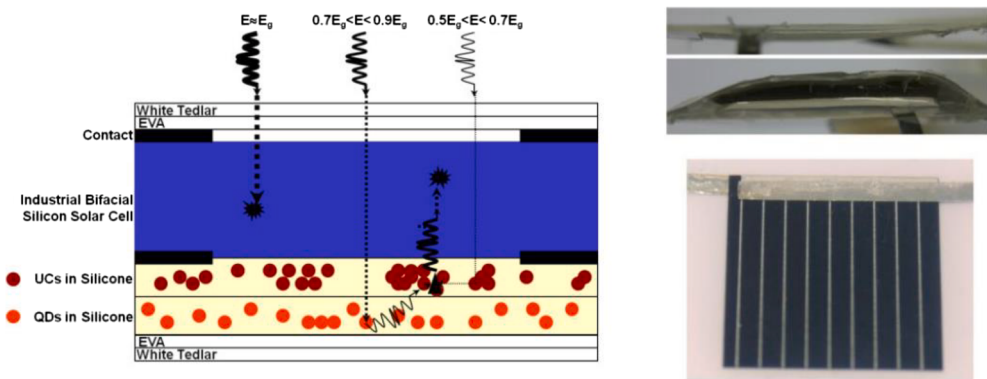


Fig. 29. Encapsulation structure of a bPV cell with UC and QDs [119].

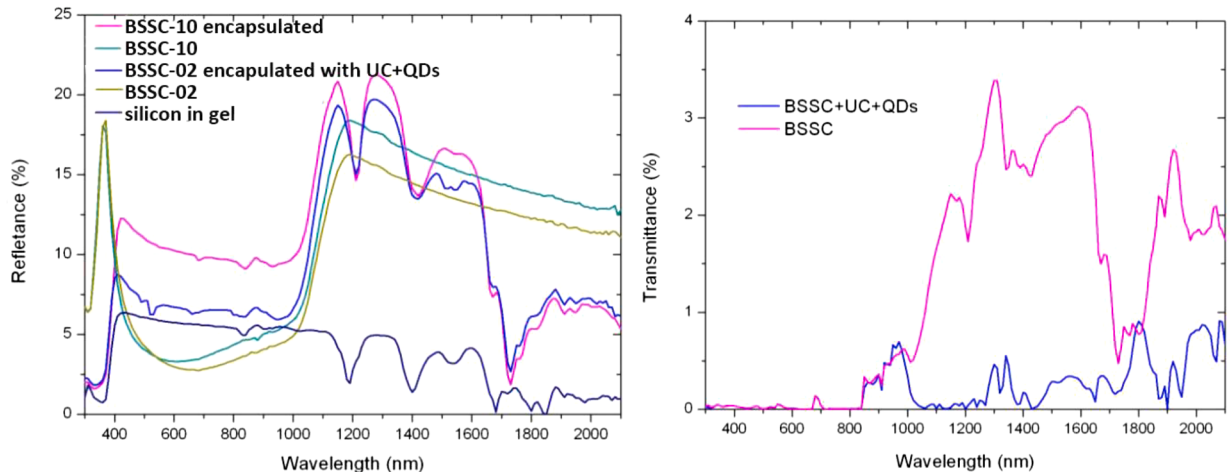


Fig. 30. Optical characterization of BSSC with and without UC and QDs [119].

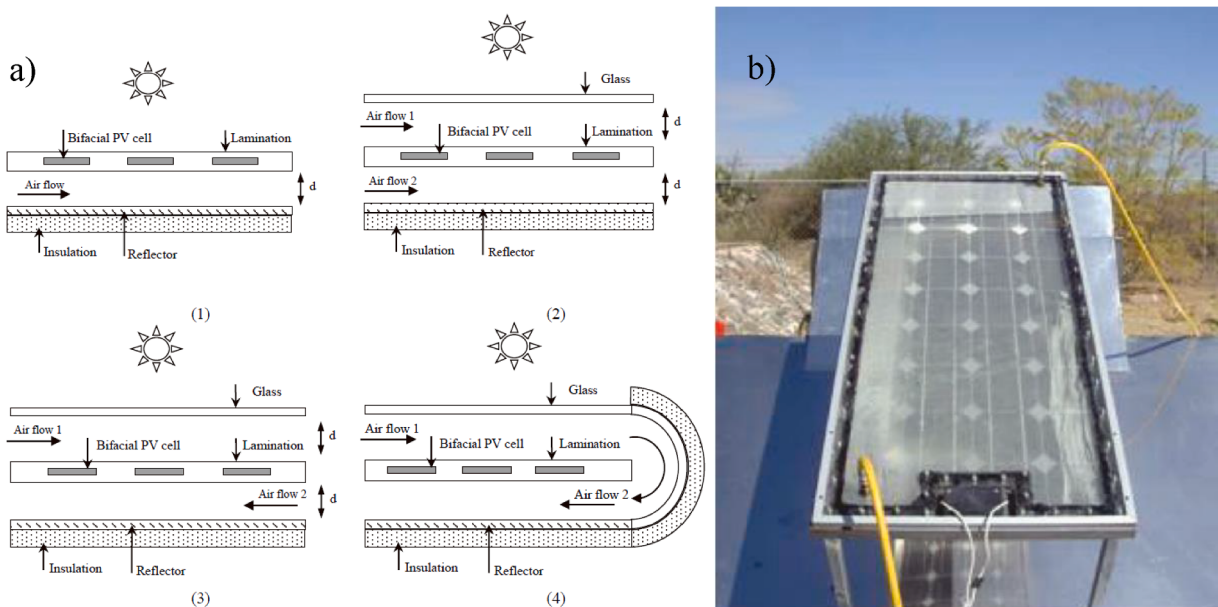


Fig. 31. Two types of bPV/T designs: a) air cooling [122]; b) water cooling [123].

will become widespread if combined with bPV technology as the attention of the market is shifted from mPV to bPV technology.

4.2.5. Revolution of module encapsulation

Tedlar and ethylene-vinyl acetate copolymer (EVA) are used as backsheet materials and cell encapsulation, when connecting many conventional PV cells in series to form a PV module. This will not be suitable in the future for bPV module encapsulation as described in Section 2.3.2 due to the many disadvantages under various conditions. Under such conditions, glass and ethylene-octene copolymer (POE) with low water vapor transmission rate and high volume resistivity are better choices to ensure a longer lifetime despite the glass backsheet's heavy weight. However, the industrial debate on whether to choose the structure of 'double glass' or 'glass-transparent organic materials' will be determined due to light weight and handy installation by the development of PV glass with thickness ≤ 2.0 mm in the future.

4.2.6. Other future perspectives

As above described, there are some other future perspectives for bPV technology in terms of modeling, experiments and applications:

- In-depth research on multi-physics modelling is necessary to understand the relationship among sunlight, electricity and heat when designing and optimizing the bPV system. This should be carefully taken into consideration to estimate the electrical and thermal performance. Based on these performance indexes, especially power output, other economic and environmental indexes, such as LCOE and greenhouse-gas payback time will be obtained accurately in the future.
- The performance of bPV modules is estimated by experiments under real-word environment, including fluctuating solar irradiance, ambient temperature and wind velocity. Therefore, more work should be conducted on evaluating the bPV performance through a long-term experiment.
- Some suggestions can be provided on loss mitigation and efficiency improvement. For instance, more module-scale MPPTs (micro inverters) are employed instead of string-level MPPTs (string inverter), and the uniform albedo and long row-to-row distance are beneficial to the uniform condition of rear irradiance. Additional similar approaches need to be further researched.
- Broad applications for bPV technology will be witnessed. For cities with high latitudes, more vertical bPV arrays will be widely used instead of mPV in the future, because of onsite weather and geographic features. For low-latitude cities, bPV modules will be recommended strongly if albedo is high, such as deserts. In addition, it may be a good choice to take hybrid deployments in bPV systems compromising economy with technical feasibility. For example, establishing mix of bPV modules facing east–west and mPV modules facing south in a bPV array.

5. Conclusions

The performance estimations and applications of bifacial photovoltaic (bPV) technology are hot topics in academia and the PV markets. Many researchers have estimated the technical and economic performance of bPV technology by various models or experiments. Results show that the specific bifacial structure of bPV modules contributes to 5–30% more power output and 0–15.6% increase in initial cost, resulting in 2–6% lower leveled cost of energy (LCOE) than mono-facial photovoltaics (mPV). To achieve high electricity production, all bPV modules should be installed in a tracking system at an optimal tilt angle with high albedo, elevation and row space. However, there are still some challenges in practical applications. Especially the non-uniform rear-side irradiance, which can result in electrical mismatch, receives increasing attention. Therefore, the simulation and measurement of non-uniform level are highlighted in bPV performance characterization

methods in literature. Moreover, some potential approaches are proposed to make bPV technology more cost-effective in terms of optimization of cells, modules, and system, such as larger cells, up conversion and down conversion. Future perspectives for bPV technology in terms of modelling, experiments and applications indicate that more research is still required for wider spread of the bPV technology.

Declaration of Competing Interest

The authors declare that they have no known competing financial interests or personal relationships that could have appeared to influence the work reported in this paper.

Acknowledgements

The authors appreciate the financial supports provided by National Natural Science Foundation of China (NSFC) through the Grant No. 51976124 and Shenzhen Technology Innovation Commission (STIC) through the Grant No. JSGG20180504165907910. The authors would also like to thank Audun Bull Kristiansen for proofreading the paper.

References

- [1] Ma T, Zhao J, Li Z. Mathematical modelling and sensitivity analysis of solar photovoltaic panel integrated with phase change material. *Appl Energy* 2018; 228:1147–58.
- [2] Pan Z, Bi Y, An L. A cost-effective and chemically stable electrode binder for alkaline-acid direct ethylene glycol fuel cells. *Appl Energy* 2020;258.
- [3] Chen Z, Chen Y, Wu L, Cheng S, Lin P, You L. Accurate modeling of photovoltaic modules using a 1-D deep residual network based on I-V characteristics. *Energy Convers Manage* 2019;186:168–87.
- [4] Ma T, Javed MS. Integrated sizing of hybrid PV-wind-battery system for remote island considering the saturation of each renewable energy resource. *Energy Convers Manage* 2019;182:178–90.
- [5] REN21. Renewables 2019 Global Status Report. Available: <<http://www.ren21.net/gsr-2019/pages/foreword/foreword/>>.
- [6] Liang TS, Pravettoni M, Deline C, Stein JS, Kopecek R, Singh JP, et al. A review of crystalline silicon bifacial photovoltaic performance characterisation and simulation. *Energy Environ Sci* 2019;12:116–48.
- [7] Katsaounis T, Kotsovos K, Gereige I, Basaheeh A, Abdullah M, Khayat A, et al. Performance assessment of bifacial c-Si PV modules through device simulations and outdoor measurements. *Renewable Energy* 2019;143:1285–98.
- [8] VDMA. International Technology Roadmap for Photovoltaic (ITRPV). Available: <<https://itrpv.vdma.org/en/>>; 2020.
- [9] VDMA. International Technology Roadmap for Photovoltaic (ITRPV). Available: <<https://itrpv.vdma.org/en/>>; 2019.
- [10] Hiroshi M. Radiation energy transducing device. US Patent; 1966.
- [11] Luque A, Ruiz J, Cuevas A, Eguren J, Agost M, Sided D, et al. Solar cells to improve static concentration. *Photovolt Sol Energy Conf.*. 1978.
- [12] Cuevas A, Luque A, Eguren J, del Alamo J. 50 Percent more output power from an albedo-collecting flat panel using bifacial solar cells. *Sol Energy* 1982;29:419–20.
- [13] Kasahara N, Yoshioka K, Saitoh T. Performance evaluation of bifacial photovoltaic modules for urban application. In: Proceedings of 3rd World Conference on Photovoltaic Energy Conversion; 2003. p. 2455–8.
- [14] Sun X, Khan MR, Deline C, Alam MA. Optimization and performance of bifacial solar modules: a global perspective. *Appl Energy* 2018;212:1601–10.
- [15] Patel MT, Khan MR, Sun X, Alam MA. A worldwide cost-based design and optimization of tilted bifacial solar farms. *Appl Energy* 2019;247:467–79.
- [16] Rodríguez-Gallegos CD, Bieri M, Gandhi O, Singh JP, Reindl T, Panda SK. Monofacial vs bifacial Si-based PV modules: which one is more cost-effective? *Sol Energy* 2018;176:412–38.
- [17] Yu B, Song D, Sun Z, Liu K, Zhang Y, Rong D, et al. A study on electrical performance of N-type bifacial PV modules. *Sol Energy* 2016;137:129–33.
- [18] Stein JS, Riley D, Lave M, Hansen C, Deline C, Toor F. Outdoor field performance from bifacial photovoltaic modules and systems. In: 2017 Ieee 44th Photovoltaic Specialist Conference (PVSC); 2017. p. 3184–9.
- [19] Wei Q, Wu C, Liu X, Zhang S, Qian F, Lu J, et al. The glass-glass module using n-type bifacial solar cell with PERT structure and its performance. *Energy Procedia* 2016;92:750–4.
- [20] Gu W, Ma T, Song A, Li M, Shen L. Mathematical modelling and performance evaluation of a hybrid photovoltaic-thermoelectric system. *Energy Convers Manage* 2019;198.
- [21] Gu W, Ma T, Li M, Shen L, Zhang Y. A coupled optical-electrical-thermal model of the bifacial photovoltaic module. *Appl Energy* 2020;258:114075.
- [22] Guo S, Walsh TM, Peters M. Vertically mounted bifacial photovoltaic modules: a global analysis. *Energy* 2013;61:447–54.
- [23] Sporleder K, Naumann V, Bauer J, Richter S, Hähnel A, Großer S, et al. Root cause analysis on corrosive potential-induced degradation effects at the rear side of bifacial silicon PERC solar cells. *Sol Energy Mater Sol Cells* 2019;201.

- [24] Carolus J, Tsanakas JA, van der Heide A, Voroshazi E, De Ceuninck W, Daenen M. Physics of potential-induced degradation in bifacial p-PERC solar cells. *Sol Energy Mater Sol Cells* 2019;200.
- [25] Barbato M, Barbato A, Meneghini M, Tavernaro G, Rossetto M, Meneghesso G. Potential induced degradation of N-type bifacial silicon solar cells: an investigation based on electrical and optical measurements. *Sol Energy Mater Sol Cells* 2017;168:51–61.
- [26] Lamers MWPE, Özkalay E, Gali RSR, Janssen GJM, Weeber AW, Romijn IG, et al. Temperature effects of bifacial modules: hotter or cooler? *Sol Energy Mater Sol Cells* 2018;185:192–7.
- [27] Hanifi H, Pfau C, Turek M, Schneider J. A practical optical and electrical model to estimate the power losses and quantification of different heat sources in silicon based PV modules. *Renewable Energy* 2018;127:602–12.
- [28] Haedrich I, Eitner U, Wiese M, Wirth H. Unified methodology for determining CTM ratios: systematic prediction of module power. *Sol Energy Mater Sol Cells* 2014;131:14–23.
- [29] Wang A, Xuan Y. A detailed study on loss processes in solar cells. *Energy* 2018; 144:490–500.
- [30] Dupré O, Vaillon R, Green MA. Physics of the temperature coefficients of solar cells. *Sol Energy Mater Sol Cells* 2015;140:92–100.
- [31] Dupré O, Vaillon R, Green MA. A full thermal model for photovoltaic devices. *Sol Energy* 2016;140:73–82.
- [32] Bhaduri S, Kottantharayil A. Mitigation of soiling by vertical mounting of bifacial modules. *IEEE J Photovoltaics* 2019;9:240–4.
- [33] Guerrero-Lemus R, Vega R, Kim T, Kimm A, Shephard LE. Bifacial solar photovoltaics – a technology review. *Renewable Sustainable Energy Rev* 2016;60: 1533–49.
- [34] Faturrochman GJ, de Jong MM, Santbergen R, Folkerts W, Zeman M, Smets AHM. Maximizing annual yield of bifacial photovoltaic noise barriers. *Sol Energy* 2018; 162:300–5.
- [35] Soria B, Gerritsen E, Lefillastre P, Broquin J-E. A study of the annual performance of bifacial photovoltaic modules in the case of vertical facade integration. *Energy Sci Eng* 2016;4:52–68.
- [36] SolarGIS. SolarGIS: solar resource maps and GIS data for 200+ countries. Available: <<https://solargiscom/maps-and-gis-data/overview>>.
- [37] Stein JS, Hansen CW, Reno MJ. Global horizontal irradiance clear sky models: implementation and analysis. Sandia Report. 2012.
- [38] Saw MH, Khoo YS, Singh JP, Wang Y. Enhancing optical performance of bifacial PV modules. In: 7th International Conference on Silicon Photovoltaics, Siliconpv 2017; 2017. p. 484–94.
- [39] Liu BYH, Jordan RC. The long-term average performance of flat-plate solar-energy collectors: with design data for the U.S., its outlying possessions and Canada. *Sol Energy* 1963;7:53–74.
- [40] Duffie JA, Beckman WA, Worek WM. Solar engineering of thermal. Process A Wiley-Interscience publication; 2006. p. 549.
- [41] Perez R, Stewart R, Arbogast C, Seals R, Scott J. An anisotropic hourly diffuse radiation model for sloping surfaces: description, performance validation, site dependency evaluation. *Solar Energy* 1986;36:481–97.
- [42] Appelbaum J. The role of view factors in solar photovoltaic fields. *Renewable Sustainable Energy Rev* 2018;81:161–71.
- [43] Sönmez FF, Ziar H, Isabella O, Zeman M. Fast and accurate ray-casting-based view factor estimation method for complex geometries. *Sol Energy Mater Sol Cells* 2019;200.
- [44] LBNL. RADIANCE software. Available: <<https://floyd.lbl.gov/radiance/framed.html>>; 1990s.
- [45] LRC. TracePro software. Available: <<https://www.lambdares.com/tracepro/>>; 2020.
- [46] Comsol. Simulate ray tracing in optically large systems with the ray optics module. Available: <<https://www.comsol.com/ray-optics-module>>; 2014.
- [47] Deline C, MacAlpine S, Marion B, Toor F, Asgharzadeh A, Stein JS. Evaluation and field assessment of bifacial photovoltaic module power rating methodologies. In: 2016 IEEE 43rd Photovoltaic Specialists Conference (PVSC); 2016. p. 3698–703.
- [48] Asgharzadeh A, Marion B, Deline C, Hansen C, Stein JS, Toor F. A sensitivity study of the impact of installation parameters and system configuration on the performance of bifacial PV arrays. *IEEE J Photovoltaics* 2018;8:798–805.
- [49] Pelaez SA, Deline C, MacAlpine SM, Marion B, Stein JS, Kostuk RK. Comparison of bifacial solar irradiance model predictions with field validation. *IEEE J Photovoltaics* 2019;9:82–8.
- [50] Shoukry I, Libal J, Kopecik R, Wefringhaus E, Werner J. Modelling of bifacial gain for stand-alone and in-field installed bifacial PV modules. *Energy Procedia* 2016;92:600–8.
- [51] Tossa AK, Soro YM, Azoumah Y, Yamegueu D. A new approach to estimate the performance and energy productivity of photovoltaic modules in real operating conditions. *Sol Energy* 2014;110:543–60.
- [52] Mermod A, Wittemer B. Yield simulations for horizontal axis trackers with bifacial PV modules in PVsyst. 35th European Photovoltaic Solar Energy Conference. 2018.
- [53] Merten J, Coignus J, Razongles G, Muñoz D. Novel equivalent circuit for heterojunction cells and diagnostic method based on Variable Illumination Measurements (VIM); 2012.
- [54] Merten J, Asensi JM, Voz C, Shah AV, Platz R, Andreu J. Improved equivalent circuit and analytical model for amorphous silicon solar cells and modules. *IEEE Trans Electron Devices* 1998;45:423–9.
- [55] Merten J, Andreu J. Clear separation of seasonal effects on the performance of amorphous silicon solar modules by outdoor I/V-measurements. *Sol Energy Mater Sol Cells* 1998;52:11–25.
- [56] Piccoli E. Modeling an innovative shading device integrating PV. Universitat Politècnica de Catalunya; 2017.
- [57] Dobos AP. An improved coefficient calculator for the California energy commission 6 parameter photovoltaic module model. *J Solar Energy Eng, Trans ASME* 2012;134.
- [58] Yordanov GH, Midtgård O-M, Saetre TO. Series resistance determination and further characterization of c-Si PV modules. *Renewable Energy* 2012;46:72–80.
- [59] Yusufoglu UA, Pletzer TM, Koduvilekulathu LJ, Comparotto C, Kopecik R, Kurz H. Analysis of the annual performance of bifacial modules and optimization methods. *IEEE J Photovoltaics* 2015;5:320–8.
- [60] Merten J, Sicot L, Delesse Y, Montagareuil AGD. Outdoor evaluation of the energy production of different module technologies. 23rd EU-PVSEC; 2008.
- [61] Bai J, Liu S, Hao Y, Zhang Z, Jiang M, Zhang Y. Development of a new compound method to extract the five parameters of PV modules. *Energy Convers Manage* 2014;79:294–303.
- [62] Humada AM, Hojabri M, Mekhilef S, Hamada HM. Solar cell parameters extraction based on single and double-diode models: a review. *Renewable Sustainable Energy Rev* 2016;56:494–509.
- [63] IEC. IEC TS 60904-1-2. Available: <<https://webstore.iec.ch/publication/34357>>.
- [64] Sandia National Laboratories. Sandia Module Temperature Model. Available: <<https://pvpmcsandia.org/modeling-steps/2-dc-module-iv/module-temperature/sandia-module-temperature-model/>>.
- [65] Sandia. Sandia National Laboratories. Sandia Cell Temperature Model. Available: <<https://pvpmcsandia.org/modeling-steps/2-dc-module-iv/cell-temperature/sandia-cell-temperature-model/>>.
- [66] Faizan D. Assessing the outdoor operating temperature of photovoltaic modules. *Prog Photovoltaics Res Appl* 2008;16:307–15.
- [67] Abotaleb A, Abdallah A. Performance of bifacial-silicon heterojunction modules under desert environment. *Renewable Energy* 2018;127:94–101.
- [68] Kutzer M, Füle A, Jahnke A, Becker J, Hahn H, Wendt S, et al. Ertragssteigerung durch bifaziale Modultechnologie; 2016.
- [69] Castillo-Aguilella JE, Hauser PS. Multi-variable bifacial photovoltaic module test results and best-fit annual bifacial energy yield model. *IEEE Access* 2016;4: 498–506.
- [70] NREL. Bifacialvf - Bifacial PV View Factor model. Available: <<https://github.com/NREL/bifacialvf>>.
- [71] Sandia. Sandia National Laboratories. PV LIB Toolbox. Available: <https://pvpmcsandia.org/applications/pv_lib-toolbox/>.
- [72] NREL. SAM 2018.11.11 for Windows. Available: <<https://samnrelgov/downloadhtml/>>; 2018.
- [73] NREL. PVsyst software v 6.78. Available: <<https://www.pvsyst.com/download/>>; 2018.
- [74] Sandia. Sandia National Laboratories. Field Example of Bifacial Gain at Sandia. Available: <<https://pvpmcsandia.gov/pv-research/bifacial-pv-project/outline-bifacial-pv-performance-data-field-example-of-bifacial-gain-at-sandia/>>.
- [75] Molin E, Stridh B, Molin A, Wackelgard E. Experimental yield study of bifacial PV modules in nordic conditions. *IEEE J Photovoltaics* 2018;8:1457–63.
- [76] Rabanal-Arabach J, Schneider A. Anti-reflective coated glass and its impact on bifacial modules' temperature in desert locations. *Energy Procedia* 2016;92: 590–9.
- [77] Singh JP, Guo S, Peters IM, Aberle AG, Walsh TM. Comparison of glass/glass and glass/backsheet PV modules using bifacial silicon solar cells. *IEEE J Photovoltaics* 2015;5:783–91.
- [78] Branker K, Pathak MJM, Pearce JM. A review of solar photovoltaic levelized cost of electricity. *Renewable Sustainable Energy Rev* 2011;15:4470–82.
- [79] Deline C, Peláez SA, Marion B, Sekulic B, Woodhouse M, Stein J. Bifacial PV system performance: separating fact from fiction. Plenary presentation at Photovoltaics Specialists Conference. 2019.
- [80] Fertig F, Nold S, Wöhrle N, Greulich J, Hädrich I, Krauß K, et al. Economic feasibility of bifacial silicon solar cells. *Prog Photovoltaics Res Appl* 2016;24: 800–17.
- [81] Tillmann P, Jäger K, Becker C. Minimising the levelised cost of electricity for bifacial solar panel arrays using Bayesian optimisation. *Sustainable Energy Fuels* 2020;4:254–64.
- [82] Van Aken BB, Carr AJ. Relating indoor and outdoor performance of bifacial modules. In: 2014 IEEE 40th Photovoltaic Specialist Conference (PVSC); 2014. p. 1381–3.
- [83] Wang S, Wilkie O, Lam J, Steeman R, Zhang W, Khoo KS, et al. Bifacial photovoltaic systems energy yield modelling. *Energy Procedia* 2015;77:428–33.
- [84] Wang L, Liu F, Yu S, Quan P, Zhang Z. The study on micromismatch losses of the bifacial PV modules due to the irradiance nonuniformity on its backside surface. *IEEE J Photovoltaics* 2019;1:9.
- [85] Kreinin L, Bordin N, Karsenty A, Drori A, Grobgeld D, Eisenberg N. PV module power gain due to bifacial design. In: Preliminary experimental and simulation data. 2010 35th IEEE Photovoltaic Specialists Conference; 2010. p. 002171–2175.
- [86] Sun L, Lu L, Yang H. Optimum design of shading-type building-integrated photovoltaic claddings with different surface azimuth angles. *Appl Energy* 2012; 90:233–40.
- [87] Lopez-Garcia J, Casado A, Sample T. Electrical performance of bifacial silicon PV modules under different indoor mounting configurations affecting the rear reflected irradiance. *Sol Energy* 2019;177:471–82.
- [88] Luque EG, Antonanzas-Torres F, Escobar R. Effect of soiling in bifacial PV modules and cleaning schedule optimization. *Energy Convers Manage* 2018;174: 615–25.

- [89] Razongles G, Sicot L, Joanny M, Gerritsen E, Lefillastre P, Schroder S, et al. Bifacial photovoltaic modules: measurement challenges. *Energy Procedia* 2016; 92:188–98.
- [90] Bhang BG, Lee W, Kim GG, Choi JH, Park SY, Ahn H-K. Power performance of bifacial c-Si PV modules with different shading ratios. *IEEE J Photovoltaics* 2019; 1–8.
- [91] De Groot KM, Van Aken BB. Near-field partial shading on rear side of bifacial modules. *Energy Procedia* 2017;124:532–9.
- [92] IEC. IEC TS 60904-1-2. Available: <<https://webstore.iecch/publication/34357>>; 2019.
- [93] Liang TS, Poh D, Pravettoni M. Challenges in the pre-normative characterization of bifacial photovoltaic modules. In: Proceedings of the 12th International Photovoltaic Power Generation and Smart Energy Conference & Exhibition (SneC2018); 2018. p. 66–73.
- [94] Bordina NM, Borisova NA, Daletskii GS, Zadde VV, Zaitseva AK, Landsman AP, et al. Using the radiation reflected from the earth for increasing the power of solar batteries. *Cosm Res* 1976;14:266–72.
- [95] Eisenberg N, Bordin N, Kreinin L, Kalikauskas VS, Zviagina KN, Kagan M, et al. Future of bifacial Si solar cells for space applications. 23rd European Photovoltaic Solar Energy Conference and Exhibition. 2008.
- [96] Prat L, Alcubilla R, Blasco E, Garcia E, Calderer J, Correig X, et al. Performance analysis of bifacial silicon solar cells in a space environment. *Solar Cells* 1990;29: 303–18.
- [97] Delleur AM, Kerslake TW. Electrical performance of the international space station US photovoltaic array during bifacial illumination. *IEEE2002*. In: *IECEC'02 2002 37th Intersociety Energy Conversion Engineering Conference*; 2002. p. 39–44.
- [98] Hokuto. Japan's Asahikawa megawatt-scale photovoltaic power station: using double-sided light-receiving panels to "turn snow into treasure". Available: <<http://wwwne21com/news/show-51711html>>; 2013.
- [99] Dongying. China's first and largest double-sided double-glass component power plant project is about to be connected to the grid. Available: <<http://www.pvmen.com/article/7666.html>>; 2018.
- [100] Wuhai. Yingli Green using bifacial modules in 100MW 'Top Runner' project. Available: <<https://www.pv-tech.org/news/yingli-green-using-bifacial-module-s-in-100mw-topper-runner-project>>; 2017.
- [101] Netherland. A major breakthrough! Europe's largest N-type double-sided solar power plant successfully connected to the grid. Available: <http://www.pv-tech.cn/news/Europe's_largest_N-type_double-sided_solar_power_plant_successfully_connect>; 2019.
- [102] US. LONGi will supply 224MW double-sided PERC components for the largest "double-sided + tracking" project in the US. Available: <http://www.pv-tech.cn/news/Longji_will_supply_224MW_double-sided_PERC_components_for_the_largest_doub>; 2019.
- [103] Traxscara. Mexico's largest bifacial photovoltaic power station. Available: <http://www.pv-tech.cn/news/Longi_and_Enel_build_Mexicos_largest_double-sided_photovoltaic_power_stat>; 2019.
- [104] Chile. World's largest bifacial PV plant nears completion in Chile. Available: <https://www.pv-tech.org/news/worlds_largest_bifacial_pv_plant_nears_compl>; 2015.
- [105] Datong. Yingli Green completes 50MW 'Top Runner' PV power plant project. Available: <<http://wwwpv-technnews/yingli-green-completes-50mw-top-runner-pv-power-plant-project>>; 2016.
- [106] Joge T, Araki I, Takaku K, Nakahara H, Eguchi Y, Tomita T. Advanced applications of bifacial solar modules. In: *3rd World Conference on Photovoltaic Energy Conversion*; 2003. p. 2451–4.
- [107] Hezel R. Novel applications of bifacial solar cells. *Prog Photovoltaics Res Appl* 2003;11:549–56.
- [108] Araki I, Tatsunokuchi M, Nakahara H, Tomita T. Bifacial PV system in Aichi Airport-site demonstrative research plant for new energy power generation. *Sol Energy Mater Sol Cells* 2009;93:911–6.
- [109] Baumann T, Nussbaumer H, Klenk M, Dreisiebner A, Carigiet F, Baumgartner F. Photovoltaic systems with vertically mounted bifacial PV modules in combination with green roofs. *Sol Energy* 2019;190:139–46.
- [110] Switzerland. World's first bifacial sound insulation system near Wallisellen/Zurich, 10 kWp pilot system. Available: <<https://www.tnc.ch/en/photovoltaics/#pv-noise-barrier>>; 1997.
- [111] Nordmann T, Goetzberger A. Motorway sound barriers: recent results and new concepts for advancement of technology; 1994.
- [112] Liang TS, Poh D, Pravettoni M. Challenges in the pre-normative characterization of bifacial photovoltaic modules. *Energy Procedia* 2018;150:66–73.
- [113] Wohrle N, Fellmeth T, Greulich J, Bitnar B, Neuhaus H, Palinginis P, et al. Understanding the rear-side layout of p-doped bifacial PERC solar cells with simulation driven experiments. In: *7th International Conference on Silicon Photovoltaics, SiliconPV 2017*; 2017. p. 225–34.
- [114] Tonini D, Cellere G, Bertazzo M, Fecchio A, Cerasti L, Galiazzo M. Shingling technology for cell interconnection: technological aspects and process integration. *Energy Procedia* 2018;150:36–43.
- [115] Beaucarne G. Materials challenge for shingled cells interconnection. *Energy Procedia* 2016;98:115–24.
- [116] Schulte-Huxel H, Blankemeyer S, Morlier A, Brendel R, Köntges M. Interconnect-shingling: maximizing the active module area with conventional module processes. *Sol Energy Mater Sol Cells* 2019;200:109991.
- [117] Yagiura T, Morizane M, Murata K, Uchihashi K, Tsuda S, Nakano S, et al. Exchangeable PV shingle. *Sol Energy Mater Sol Cells* 1997;47:227–33.
- [118] Green MA. Third generation photovoltaics: advanced solar. *Energy Convers* 2006.
- [119] Pan AC, Zanesco I, Moehlecke A. Industrial bifacial silicon solar cells with up-converter and PbS quantum dots. *Energy Procedia* 2014;44:160–6.
- [120] Pan AC, Cardoso LSG, Reis FSd. Modeling mathematical of the behavior of up converter when implemented in bifacial silicon solar cells. *Energy Procedia* 2016; 102:80–6.
- [121] Trupke T, Green MA, Würfel P. Improving solar cell efficiencies by down-conversion of high-energy photons. *J Appl Phys* 2002;92:1668–74.
- [122] Oshakhsaraei P, Sopian K, Zaidi SH, Zulkifli R. Performance of four air-based photovoltaic thermal collectors configurations with bifacial solar cells. *Renewable Energy* 2017;102:279–93.
- [123] Robles-Ocampo B, Ruiz-Vazquez E, Canseco-Sánchez H, Cornejo-Meza RC, Trápaga-Martínez G, García-Rodríguez FJ, et al. Photovoltaic/thermal solar hybrid system with bifacial PV module and transparent plane collector. *Sol Energy Mater Sol Cells* 2007;91:1966–71.
- [124] Al-Rousan N, Isa NAM, Desa MKM. Advances in solar photovoltaic tracking systems: a review. *Renewable Sustainable Energy Rev* 2018;82:2548–69.